

SMART SENSORS AND THEIR APPLICATION IN MONITORING RESPIRATORY RATE

Bachelor thesis

Study programme: B3944 - Biomedical Technology
Study branch: 3901R032 - Biomedical Technology

Author: Wusu Sorie Nanday Kamara
Supervisors: Prof. Ing. Jaroslav Nosek, CSc.

Liberec 2020

INTELIGENTNÍ SENZORY A JEJICH APLIKACE PRO MONITOROVÁNÍ RESPIRAČNÍCH POMĚRŮ

Bakalářská práce

Studijní program: B3944 - Biomedicínská technika
Studijní obor: 3901R032 - Biomedicínská technika

Autor práce: Wusu Sorie Nanday Kamara
Vedoucí práce: Prof. Ing. Jaroslav Nosek, CSc.

Liberec 2020

© **Technická univerzita v Liberci, 2020**
ISBN 978-80-7494-317-1

Zadání bakalářské práce

**Smart sensors and their application in
monitoring respiratory rate**

Jméno a příjmení: **B.Sc. Wusu Sorie Nanday Kamara**
Osobní číslo: **D18000108**
Studijní program: **B3944 Biomedicínská technika**
Studijní obor: **Biomedicínská technika**
Zadávající katedra: **Fakulta zdravotnických studií**
Akademický rok: **2019/2020**

Zásady pro vypracování:

Cíle práce:

1. Research of currently published results in monitoring respiratory rate (MRR). The work will be focused on the Respiratory Inductive Plethysmography (RIP), using different types of intelligent sensors of the respiratory pressure (PI).
2. Comparison of properties of selected intelligent respiratory pressure sensors suitable for MRR.
3. Piezoelectric sensors based on relaxor materials. Conceptual design of the sensor.
4. Laboratory realization of the sensor for monitoring respiratory pressure and its application. Signal processing and signal evaluation.

Teoretická východiska (včetně výstupu z kvalifikační práce):

The student will be acquainted with the possibilities of respiratory monitoring by RIP methodology, especially with the implementation of piezoelectric respiratory pressure sensors and subsequent signal processing. Student designs a solution that uses smart materials to significantly increase the sensitivity of the respiratory pressure sensor (although these materials are not readily available). The student will perform basic measurement of respiratory pressure.

Výzkumné předpoklady / výzkumné otázky:

The research prerequisite is a good knowledge of the physical principles of piezoelectric, piezoresistive and capacitive sensors suitable for sensing of the respiratory pressure. At the same time, the application possibilities of placing these sensors on the patient's body and outside the patient will be studied. Based on the comparison of properties of the respiratory pressure sensors (of different physical principles and possible applications), the student will design a simple respiratory pressure sensor.

Metoda:

This work has a quantitative character.

Technika práce, vyhodnocení dat:

The theoretical output of the work will be verified on the respiratory instrument in the Physical Measurement Department at CxI.

Místo a čas realizace výzkumu:

TUL-Faculty of Mechatronics, Informatics and Interdisciplinary Studies and Department of Physical Measurements at the Institute for Nanomaterials, Advanced Technologies and Innovation (CxI) are the places for the realization of the qualification work.

1. Research part – 8.1.2020,
2. Comparison of properties of respiratory pressure sensors and their location. Conceptual sensor design based on relaxor materials -15.2.2020,
3. Realization of respiratory pressure sensor and its laboratory application – 15.4.2020,
4. Processing of results and first version of the qualification work – 15.5.2020,
5. Final version of the work -26.6.2020.

Vzorek:

Due to the qualitative nature of the work, the sample of respondents will not be used.

Rozsah práce:

The range of bachelor thesis is 50-70 pages.

Forma zpracování kvalifikační práce:

A printed and electronic form of the work.

Seznam odborné literatury:

1. KLAP, Tal a Zvika SHINAR. Using piezoelectric sensor for continuous-contact-free monitoring of heart and respiration rates in real-life hospital settings. *Computing in Cardiology Conference (CinC)*, 2013. **40**, 671-674, ISBN:978-1-4799-0884-4
2. KOŤOVÁ, M. Monitorování dechu během terapie pacientů. Diplomová práce VUT FEKT Brno, 2013. https://www.vutbr.cz/www_base/zav_prace_soubor_verejne.php?file_id=64651
3. SETTER, N., Ed., *Piezoelectric materials in devices*, Ceramic Laboratory, Swiss Federal Institute of Technology (EPFL) Lausanne, Swiss, 2002. ISBN 2-9700346-0-3, EAN 9782970034605.
4. RUPITSCH, Stefan. *J. Piezoelectric Sensors and Actuators*. Berlin, Heidelberg: Springer Berlin Heidelberg, 2019. Topics in Mining, Metallurgy and Materials Engineering. ISBN 978-3-662-57532-1
5. MANJUNATHA, Roopa. G. et al. Identification of different respiratory rate by a piezo polymer based nasal sensor. In: *2013 IEEE SENSORS*. IEEE, 2013, s. 1-4. DOI 10.1109/ICSENS.2013.6688479. Dostupné také z: <http://ieeexplore.ieee.org/document/6688479>
6. HAMDANI, Syed a Anura FERNANDO. The Application of a Piezo-Resistive Cardiorespiratory Sensor System in an Automobile Safety Belt. *Sensors*. 2015, **15**(4), 7742-7753 [cit. 2018-12-19]. DOI 10.3390/s150407742. ISSN 1424-8220. Dostupné také z: <http://www.mdpi.com/1424-8220/15/4/7742>
7. YU-PEI HUANG a KE-NUNG HUANG. Monitoring of breathing rate by a piezofilm sensor using pyroelectric effect. In: *2013 1st International Conference on Orange Technologies (ICOT)*. IEEE, 2013, s. 99-102. DOI 10.1109/ICOT.2013.6521167. Dostupné také z: <http://ieeexplore.ieee.org/document/6521167/>
8. SUN, Xiao, et al. Sleep monitor: Monitoring respiratory rate and body position during sleep using smartwatch. *Proceedings of the ACM on Interactive, Mobile, Wearable and Ubiquitous Technologies*, 2017, **1**(3) 104. DOI: 10.1145/3130969. Dostupné také z: <http://dl.acm.org/citation.cfm?doid=3139486.3130969>.
9. SHANKAR, N. et al: Measurement of Respiratory Rate Using Piezoelectric Sensor, *Int. J. Scientific Research and Review*, vol.7, 1,2018, 184-188, ISSN 2279-543X.
10. Piezoelectric Respiration (PZT), Sensor Data Sheet. http://bitalino.com/datasheets/PZT_Sensor_Datasheet.pdf (12/2018)
11. LUIS, Juan et al. Design and Implementation of a Smart Sensor for Respiratory Rate Monitoring. *Sensors*. 2014, **14**(2), 3019-3032. DOI 10.3390/s140203019. Dostupné také z: <http://www.mdpi.com/1424-8220/14/2/3019>.

Vedoucí práce:

prof. Ing. Jaroslav Nosek, CSc.
Ústav mechatroniky a technické informatiky

Datum zadání práce:

2. září 2019

Předpokládaný termín odevzdání: 30. června 2020




prof. MUDr. Karel Cvachovec, CSc., MBA
děkan

V Liberci dne 31. ledna 2020

Declaration

I hereby certify that I have written this bachelor thesis as an original and primary work using the literature listed below and consulting it with my thesis supervisor.

I acknowledge that my bachelor's thesis is fully governed by Act No. 121/2000 Coll., the Copyright Act, in particular, Article 60 – School Work.

I acknowledge that the Technical University of Liberec does not infringe on my copyrights by using my bachelor thesis for the internal purpose of the Technical University of Liberec. I am aware of my obligation to inform the Technical University of Liberec on having used or granted a license to use the results of my bachelor thesis; in such a case the Technical University of Liberec may require reimbursement of the costs incurred for creating the results up to their actual amount.

At the same time, I honestly declare that the text of the printed version of my bachelor thesis is identical with the text of the electronic version up-loaded into the IS/STAG. I acknowledge that the Technical University of Liberec will make my bachelor thesis public by following paragraph 47b of Act No. 111/1998 Coll., on Higher Education Institutions and Amendment to Other Acts (the Higher Education Act), as amended.

I am aware of the consequences which may under the Higher Education Act result from a breach of this declaration.

Acknowledgement

Thanks to God, my Lord, and saviour Jesus Christ, for his guidance and protection throughout this journey, in my lost times and for giving me the courage to pursue my dreams.

I would also like to express my sincere gratitude to the Faculty of Health Studies at the Technical University of Liberec TUL, for the opportunity to fulfil my goal in studying biomedical technology.

I wish to thank my supervisor Prof. Ing. Jaroslav Nosek, CSc, in the Faculty of Mechatronics, Informatics and Interdisciplinary Studies, Institute of Mechatronics and Computer Engineering, for his enormous patience and guidance he has given me throughout this process. I also want to express my thanks and appreciation to Martin Pustka PhD, at the Measurement, Analysis and Reduction of Noise and Vibration Department at VÚTS Liberec, for facilitating the experimental process of this thesis.

My sincere appreciation also goes to my family both in Sierra Leone and the United Kingdom, for their unconditional love and endless support throughout my academic pursuit. To my mother, Gloria Mabinti Fallah, you have always been exceptional. Thank you for your unwavering support every step of the way. I appreciate everything you have done for me.

Last but not least, thank you to my good friends, who make life fun and worth living.

Annotation

AUTHOR:	BSc. Wusu Sorie Nanday Kamara
INSTITUTION:	Technical University of Liberec, Faculty of Health Studies – Biomedical Technology
THESIS TITLE:	Smart sensors and their application in monitoring respiratory rate
SUPERVISOR:	Prof. Ing. Jaroslav Nosek, CSc.
PAGES:	83
APPENDIX:	3
YEAR:	2020

ANNOTATION:

This bachelor thesis focuses on determining the sensitivity and design of a smart sensor that could be used in a device for the monitoring of respiratory rate with the help of respiratory inductive plethysmography (RIP). RIP is a method for monitoring respiratory rate by using a respiratory belt to which smart sensors are attached and surrounding it to the thoracic region and abdomen of a patient. An extensive literature search on piezoelectric materials that would be suitable for a smart sensor of physical forces, especially in the low-frequency range, was performed. A force sensor was designed based on PZT considering the transducer of large Force (caused by changes in chest wall movement) to the compressive Force measured by the piezoelectric sensor, was considered. Two types of piezoelectric materials were experimentally studied: PZT soft ceramics and α -Quartz. The piezoelectric coefficient for Quartz modification α was verified experimentally in the dynamic model. The measurement of the output charge Q of the sensor, using the circuit with a very large input impedance, was discussed.

From all indications, the Quartz α is more suitable than soft PZT in terms of sensor signal quality. Considerable attention was given to the more recent relaxor materials, which show an extremely high coefficient of electromechanical coupling. However,

their availability is limited. The scope of the experimental work was limited by measures against the spread of coronavirus in the period from March to May 2020, as the VÚTS and CxI laboratories were on quarantine.

KEYWORDS: Respiratory rate measurement; piezoelectric materials; piezoelectric sensor

Anotace

- AUTOR:** BSc. Wusu Sorie Nanday Kamara
- INSTITUCE:** Technická univerzita v Liberci, Fakulta zdravotnických Studií – Biomedicínská technika
- NÁZEV PRÁCE:** Inteligentní sensory a jejich aplikace pro monitorování respiračních poměrů
- VEDOUcí PRÁCE:** Prof. Ing. Jaroslav Nosek, CSc.
- POČET STRAN:** 83
- POČET PŘÍLOH** 3
- ROK OBHAJOBY:** 2020

SOUHRN:

Tato bakalářská práce je zaměřena na návrh senzitivita inteligentního senzoru pro monitorování respiračních poměrů pomocí respirační induktivní pletysmografie (RIP). RIP je metoda pro monitorování dýchacích poměrů pomocí dýchacího pásu, ke kterému jsou připojeny inteligentní senzory a obklopují jej v oblasti hrudníku a břicha. Byla provedena rozsáhlá literární rešerše piezoelektrických materiálů, které by byly vhodné pro inteligentní senzor fyzikálních sil, zejména v nízkofrekvenčním rozsahu. Senzor síly byl navržen na základě piezoelektrické keramiky typu PZT. Byl uvažován převodník roztažné síly (způsobené změnou obvodu hrudníku) na tlakovou sílu, měřenou piezoelektrickým senzorem. Experimentálně byly zkoumány dva typy piezoelektrických materiálů: měkká keramika PZT a křemen modifikace α . Piezoelektrický koeficient pro modifikaci křemene α byl experimentálně ověřen v dynamickém režimu. Bylo diskutováno měření výstupního náboje Q snímače pomocí obvodu s velmi vysokou vstupní impedancí.

Ukázalo se, že křemen α je vhodnější než keramika PZT, pokud jde o kvalitu signálu senzoru. Pozornost byla věnována také novým relaxorovým materiálům, které vykazují extrémně vysoký koeficient elektromechanické vazby. Jejich dostupnost je však omezená. Rozsah experimentální práce byl omezen z důvodu opatření proti šíření

koronaviru v období od března do května 2020, protože v laboratořích VÚTS a CxI na univerzitě byly karantény.

KLÍČOVÁ SLOVA: měření respiračních poměrů; piezoelektrické materiály;
piezoelektrický senzor

Table of Contents

Table of Contents

SMART SENSORS AND THEIR APPLICATION IN MONITORING RESPIRATORY RATE.....	1
INTELIGENTNÍ SENZORY A JEJICH APLIKACE PRO MONITOROVÁNÍ RESPIRAČNÍCH POMĚRŮ	2
Declaration.....	7
Acknowledgement	8
Annotation.....	9
Anotace	11
List of abbreviations	15
1. INTRODUCTION	16
1.1 Background.....	16
1.2 Purpose of the study.....	19
1.3 Overview of work	19
2. THEORETICAL PART.....	20
2.1 Physiology of respiration	20
2.1.1 Respiratory muscles	21
2.1.2 Mechanism of breathing.....	21
2.2 Monitoring of respiratory rate (MRR)	24
2.3 Comparison of properties of selected respiratory pressure sensors for MRR 26	
2.3.1 Acoustic pressure sensors	26
2.3.2 Fibre-optic pressure sensors (FOS).....	27
2.3.3 Resistive pressure sensors.....	28
2.3.4 Capacitive pressure sensors	29
2.3.5 Schematic comparison	30
3. PIEZOELECTRIC SMART MATERIALS.....	33
3.1 Characterisation of relaxor based materials	33
3.1.1 Overview of typical ferroelectrics and relaxor ferroelectrics.....	33

3.1.2	Morphotropic phase boundary (MPB) and Domain structure of ceramic materials	36
3.1.3	Relaxor-based Ferroelectrics and its properties	38
3.2	Conceptual design of the sensor.....	42
3.2.1	Piezoelectric sensor.....	43
3.2.2	Structural arrangement in a piezoelectric quartz crystal	44
3.2.3	Force and pressure response in piezoelectric sensor.....	50
3.2.4	Design of the piezoelectric sensor based on the PZT	51
4.	EXPERIMENTAL PART.....	54
4.1	Piezoelectric properties of the PZT ceramics.....	54
4.2	Laboratory verification of the basic properties of selected smart materials.....	55
4.2.1	Sample materials tested.....	55
4.2.2	Measurement chain	55
4.2.3	Operation of the charge amplifier	56
4.2.4	The methodology of Calibrated systems.....	57
4.2.5	Experimental result	61
4.3	Signal processing and signal evaluation	63
4.4	Experimental analysis	64
4.4.1	Results analysis.....	64
4.4.2	Limitations	65
5.	DISCUSSION.....	66
6.	CONCLUSION.....	68
	Future work.....	69
	References.....	70
	Appendix.....	78
	List of figures.....	82
	List of tables.....	83

List of abbreviations

HR	Heart Rate
DBMS	Database Management System
HIS	Hospital Information System
MRI	Magnetic Resonance Imaging
SPECT	Single Photon Emission Computed Tomography
BP	Blood Pressure
RR	Respiratory Rate
rHRV	Respiratory Induced Heart variability
PFT	Pulmonary Function testing
NP	Nasal Prongs
EIP	Electric impedance Plethysmography
OEP	Optoelectronic Plethysmography
RIP	Respiratory Inductive Plethysmography
CO₂	Carbon dioxide
O₂	Oxygen
SIDS	Sudden Infant Death Syndrome
COPD	Chronic Obstructive Pulmonary Syndrome
MRR	Monitoring of Respiratory Rate
RRa	Acoustic Respiratory Rate
FOS	Fibre Optic Sensor
FBG	Fibre Bragg Grafting
T_c	Curie Temperature
POF	Polymeric Optical Fibre
PNR	Polar Nanoscale Region
MPB	Morphotropic Phase Boundary
RUS	Resonant Ultrasound Spectroscopy
SSR	Steady-State Response
TSR	Time State Response
FFT	Fast Fourier Transformation
PZT	Lead Zirconate Titanate
PMN	Lead Magnesium Niobate
PLZT	Lead lanthanum Zirconate Titanate
PZN	Lead Zinc Niobate
PT	Lead Titanate
PZN-PT	Lead Zinc Niobate - Lead Titanate
PMN-PT	Lead Magnesium Niobate - Lead Titanate

1. INTRODUCTION

1.1 Background

Biomedical scientists and engineers have shown to bridge the gap between medicine and technology, which often involves the application of engineering knowledge and skills into the medical field. It has led to the development of devices and software to improve healthcare. Such developments could be seen in the hospital's use of database systems (DBMS, HIS) for storage of patient's information, imaging techniques like MRI, SPECT, ultrasound to name but few used in diagnostic testing. We have also seen the use of devices like spirometer, oximeter, ventilators, and many more for testing and monitor the vital function in patients including heart rate (HR), respiratory rate (RR), blood pressure (BP) body temperature, serum levels and many more. The monitoring of these parameters is essential both in healthy individuals and the patient's critical condition.

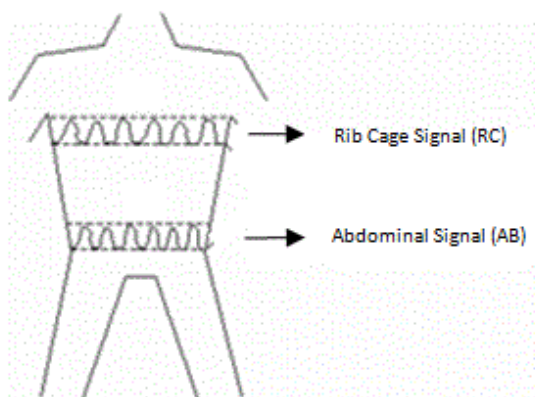
RR is one of the vital physiological parameters monitored in patients. Respiratory failure can be challenging to predict, and therefore, the monitoring of respiratory rate (MRR) is essential in the detection and diagnosis of diseases or any underlying illness and to a more considerable extent in the prevention of sudden death. RR is a measure of the number of breaths per min. According to 1993 studies done by Fieselmann, J. F et al., [1] they stated that a RR higher than 27 breaths/min is an indicator of cardiopulmonary arrest. In another research [2] in which 1695 acute patients were studied to know the effect of introducing the modified early warning score on clinical outcomes, cardio-pulmonary arrests, and intensive care utilisation in acute medical admissions, they confirmed from data analysis that RR is the best discriminator in identifying high-risk patients and early Warning score > 4 were immediately referred for urgent medical and critical care. Furthermore, in a 2017 study done on 30 critically ill and 23 brain dead patients by Jurak P et al., [3] in which their respiratory induced heart variability (rHRV) was analysed and concluded that there was a significant

difference during slow breathing at 6 to 8 breaths per min between a critically ill and brain dead patients hence indicating the importance of MRR.

The spirometer is the desired tool used for pulmonary function testing (PFT). However, researches have studied several other methods that can accurately monitor RR from isolated parts of the body such as in assessing nasal airflow (nasal prongs (NP) [4], PVDF Nasal sensor [5]), thoracic and abdomen movement (electric impedance plethysmography (EIP), optoelectronic plethysmography (OEP), respiration inductive plethysmography (RIP) [6]), and also through visual observation. The use of wearable sensors has also been studied, exploring how intelligent sensors could be used in monitoring vital function, including RR. Sensor studies for RR monitoring include the use of pressure sensors in monitoring breathing [6], piezo-polymer based nasal sensor [7], piezo-resistive cardiorespiratory sensor [8]. M. Folke et al. critically reviewed non-invasive respiratory monitoring in medical care [9], another study determines the effectiveness of the current devices of respiratory physiotherapy [10].

Piezo-resistive materials displacement sensor [11] uses sensors that can detect slight changes in pressure. RIP is a non-invasive but contact-based method that does not require a face mask or mouthpiece to monitor pulmonary ventilation by measuring the rate of movement by the chest wall and abdominal cavity. It uses smart sensors that can detect stress and strain from a patient by wrapping a stretchy flexible band that could record generated signals, rib cage signal around the chest and abdominal signals from the abdominal region as shown in figure 1. Signals detected from changes in the chest wall and abdominal displacement are analysed to determine the RR. Diaphragmatic breathing is the most important of localised breathing in athletes [6] and plays a significant role in breath control in athletes. RIP, in comparison with other techniques, has the advantage of accuracy, sensitivity, patient safety, and it has widely been used in clinical and research settings [11, 12]. It allows for the evaluation of major respiratory parameters (tidal volume, inspiration, expiration) but can be limited by the contamination of movement from other parts of the body.

Figure 1: Respiratory inductive plethysmography



Different sensors can be used in measuring the flow of inhaled and exhaled air during breathing. Kot'ová et al., studied RIP using pressure sensors that detect the changes in pressure exerted by chest wall movement during breathing [6]. From [8], they studied the application of piezo-resistive cardiorespiratory sensor system in an automobile safety belt. Even though stable respiratory signals were detected from the abdomen of the test subjects, but the measurement of signals had massive interference from heart and motion artefacts. However, through signal processing, these signals could be cancelled using filtering techniques [13]. A group of researchers [11] in a 2012 study, developed a RIP model with features supporting multiple inductive sensors by the method of inductance measurement without using a variable frequency LC oscillator. They accomplished this by further integrating pulse amplitude modulation and time division multiplexing scheme into a module to support the multiple RIP sensors [11]. It is possible to compare several methods with RIP. From [5] compared the PVDF nasal sensor for identifying RR with RIP and NP. They concluded a little to no significant difference between the different methods of measurement. In another study, [14] aimed at describing and validating a new RIP method, relying on a combination of thoracic RIP and nasal pressure signals taking into account that exercise-induced body movements can easily contaminate RIP thoracic signals by generating tissue motion artefacts. They aimed at developing a method that would facilitate the use of RIP during physical activities, thereby designing a time-domain algorithm that can distinguish between artefact and respiratory signals.

1.2 Purpose of the study

The purpose of this study is to test and determine the sensitivity of a smart material that could be used in the design and construction of a device for MRR by the method of respiratory inductive plethysmography (RIP). RIP is a method for monitoring respiratory rate by using a respiratory belt to which smart sensors are attached and surrounding it to the thoracic region and abdomen.

Piezoelectric materials are smart materials that can create a piezoelectric effect. Selected materials from this group of smart material will be tested for this project.

The overall proposed design for this project may require determining the most suitable smart material that could best fit the design of a respiratory belt, which may act as an alternative for the monitoring of RR signals in patients. This could be of enormous importance for lung functioning tests, especially during this unfortunate period of the coronavirus pandemic, that is specifically affecting the breathing pattern of infected patients. Hence, indicating the need for an alternative in MRR.

1.3 Overview of work

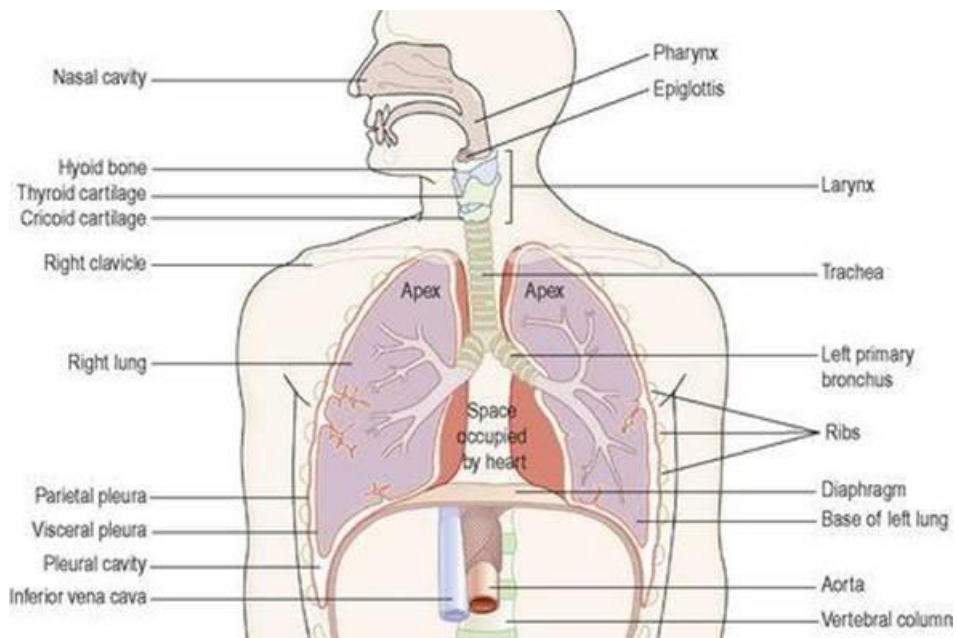
The structure of this work is presented in six (6) chapters. Chapter 1 gives a general introduction and research on currently published results in monitoring respiratory rate focusing on techniques of respiratory inductive plethysmography (RIP) using different intelligent sensors. Chapter 2 details the theoretical part of the physiology of respiration and breathing mechanism, also comparing the properties of selected intelligent pressure sensors detailing their structural composition, design, and functionality. Chapter 3 focuses on the experimental theory and properties of piezoelectric smart sensors focusing on relaxor materials and conceptual design of the sensor. Chapter 4 details the laboratory testing of sensors that could be used as an alternative for MRR, its application, experimental analysis, signal processing, and evaluation. Chapter 5 details the discussion on the acquired result while chapter 6 gives a conclusion, recommendations, and possibly future research work.

2. THEORETICAL PART

2.1 Physiology of respiration

The respiratory system is a biological system of the body consisting of the respiratory tract and its supporting structures, responsible for the exchange of gases externally and internally. External respiration involves the inhalation of oxygen O_2 through the nostril to the lungs, and the reverse is true for exhalation of carbon dioxide CO_2 . This process is known as breathing which is an active process that requires contraction of the external intercostal muscles located between the rib and the diaphragm. On the other hand, Internal respiration deals with the exchange of gases between the cells and blood capillaries. Anatomically the respiratory tract is divided into the upper airways (nose, sinuses, nasal cavities, pharynx, and upper parts of the larynx) and the lower airways (lower parts of the larynx, trachea, bronchi, bronchioles and the alveoli which are the site of gaseous exchange). Figure 2 displays the respiratory system and its associated structures.

Figure 2: Structures associated with the respiratory system. [15]



2.1.1 Respiratory muscles

The work of breathing is supported by the surrounding muscular framework of the chest and abdomen, which includes the diaphragm, intercostal muscles of the ribs, abdominal muscles, and neck muscles. These muscles enable and support the entire involuntary breathing process. The diaphragm is the most important inspiratory muscle and separates the thorax and abdominopelvic cavities. As seen in Figure 2, it has a dome-shaped when relaxed, pierced by the aorta, inferior vena cava, and oesophagus [16].

2.1.2 Mechanism of breathing

Breathing is an automatic and involuntary function but a complex process that is controlled by the respiratory centre in the hindbrain. The Medulla, which is a part of the brain stem together with its other functions, regulates all involuntary life functions, including HR, swallowing, and breathing. Breathing is the gaseous exchange of gases and is the principal purpose of the respiratory system, which involves changes in volume and pressure in the thoracic cavity. To best describe the mechanism of breathing through a gaseous exchange, it is essential to understand how pressure and volume enable breathing. It can best be described using Boyle's law which states that provided the temperature of a gas remains constant, the pressure (P) of a given mass of gas is inversely proportional to its volume (V) as shown in Eq 1. Boyle's discovered that the pressure is inversely proportional to the volume; hence, pressure increases with a decrease in the volume and vice versa. Figure 3 shows a graphical representation of the relationship between pressure and volume, as described in Boyles law. Therefore, as the lungs expand with an increase in the volume of air, the pressure within it declines. When the pressure within the lungs is less than the air pressure outside, the external air pressure will rush into the lungs, as air along with other gases flows from a region of higher pressure to a region of lower pressure.

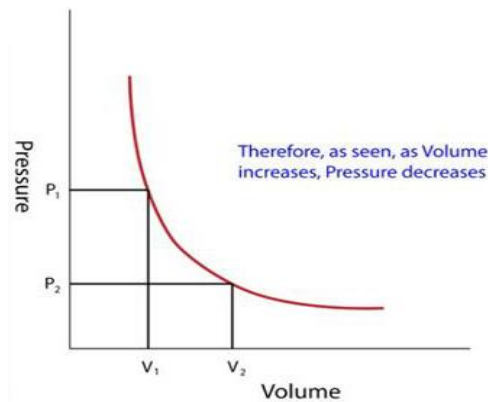
For an enclosed gas, at constant temperature T ,

$$p \propto \frac{1}{V} \quad (1)$$

$$P \propto V = \text{constant}$$

$$i. e \quad P_1V_1 = P_2V_2$$

Figure 3: Graphical description of Boyle's law



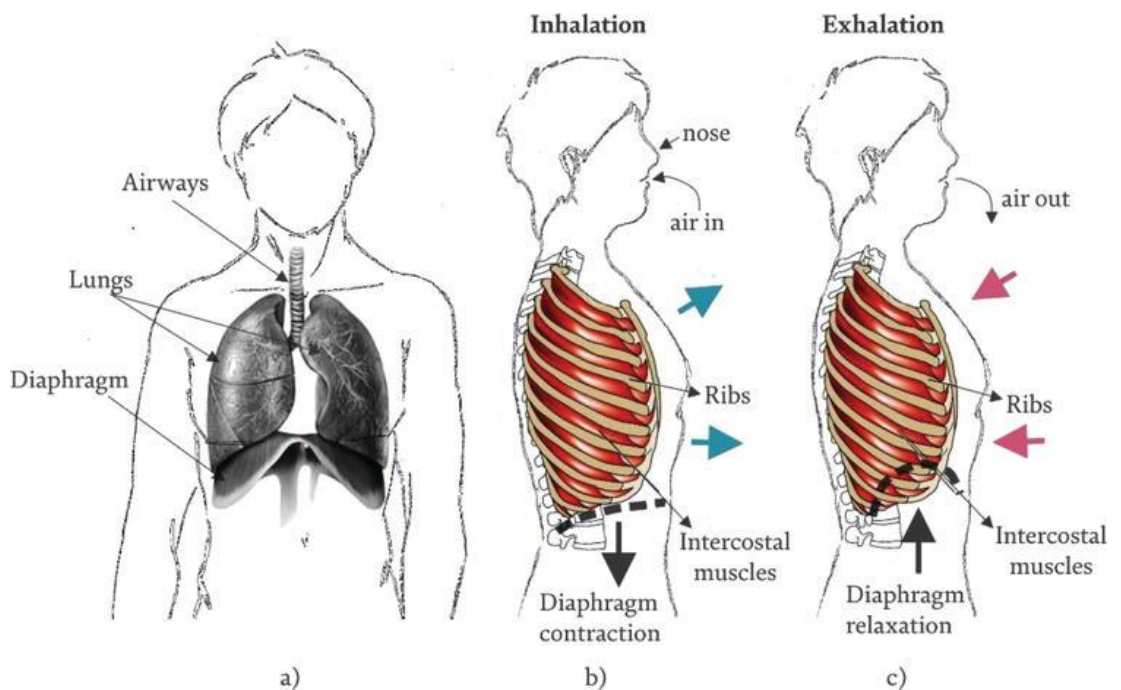
Through the principle of Boyle's law, we can see that inspiration (breathing in) and expiration (breathing out) are dependent primarily on the change in pressure between the lungs and that of the atmosphere. Three different pressures are responsible for pulmonary ventilation, and they include:

- I. Atmospheric pressure
- II. Intraalveolar (intrapulmonary) pressure
- III. Intrapleural pressure

The air pressure outside the body is known as atmospheric pressure, and it has a value of 760 mmHg [17]. The pressure within the alveolar of the lungs is called the intrapulmonary pressure, which complements the atmospheric pressure. On the other hand, intrapleural pressure refers to the pressure within the pleural cavity. During inspiration, the diaphragm contracts and the thoracic cavity increases in volume, causing a decrease in the intraalveolar pressure so that air flows into the lungs.

Figure 4a shows the structure of the airway, lungs, and diaphragm. Inspiration mechanics, as seen in figure 4b, requires the use of muscles of the diaphragm and external intercostal muscles. Breathing in (inspiration) takes air into the lungs and increase the lung volume (intrapulmonary volume). This process will cause the diaphragm and the intercostal muscles to contract, leading to an outward movement of the rib cage. An increase in the intrapulmonary volume during inhalation will decrease the intrapulmonary pressure. Figure 4c describes expiration which follows immediately after inspiration. In this situation, there is relaxation of the diaphragm and the external intercostal muscle. It will result in the diaphragm moving back to its original position, causing a decrease in the intrapulmonary volume with an increase in the intrapulmonary pressure.

Figure 4: Breathing process: (a) structures involved in the breathing process; (b) inhalation event; and (c) exhalation event. [18]










2.2 Monitoring of respiratory rate (MRR)

The MRR in patients is of great importance. Evidence-based research shows obstruction in respiratory rate as an early indicator of physiological deterioration [19] hence an easy predictor of medical complications. It plays a fundamental role in the early detection of risk factor especially in anaesthetised patients [20], Sudden Infant Death Syndrome (SIDS) in infants [21], patients with sleep apnea [22], respiratory depression in post-surgical patients [23] while obstruction of the airway such as asthma, emphysema and chronic obstructive pulmonary disease COPD will increase RR causing tachypnea [24].

Due to the importance of MRR, different methods have been established in monitoring the rate of respiration. These methods are generally classified into contact-based and contactless [25, 26]. The contact-based method (respiration inductive plethysmography, impedance plethysmography, optoelectronic plethysmography) can be invasive or non-invasive. It may require the use of a sensing device (or part of the instrument containing it) attached to the subject's body. Massaroni et al. [25] taxonomically distinguished the different available contact-based techniques for monitoring respiratory rate, as shown in Figure 5.

Figure 5: Most popular contact-based techniques for measuring RR and related areas of the body on which the sensors must be positioned. PPG = photoplethysmography; ECG = Electrocardiography. [25]

Contact-based Techniques						
Respiratory airflow	Respiratory sounds	Air Temperature	Air Humidity	Air components	Chest wall movements	Modulation cardiac activity
Flow measurements	Acoustic measurements	Temperature measurements	Relative humidity measurements	CO ₂ measurements	Strain measurements	Biopotential measurements
Differential flowmeters	Microphones	Thermistors	Capacitive sensors	Infrared sensors	Resistive sensors	ECG sensors
Turbine flowmeters		Thermocouples	Resistive sensors	Fiber optic sensors	Capacitive sensors	Light intensity measurements
Hot wire anemometers		Pyroelectric sensors	Nanocrystal and nanoparticles sensors		Inductive sensors	Light intensity measurements
Fiber optic sensors		Fiber optic sensors	Fiber optic sensors		Fiber optic sensors	PPG sensors
						Impedance measurements
					Trans thoracic impedance sensors	
					Movement measurements	
					Accelerometers	
					Gyroscopes	
					Magnetometers	
						

With the contactless approach (structured light plethysmography), monitoring is performed by an instrument that does not make any contact with the subject [25, 26]. The respiratory state of a patient can be analysed using different physiological parameters such as the tidal volume, chest movement, degree of oxygen in the blood, etc. D'Angelo et al. 2008 [27] described oxygenation as the degree to which the body utilises the oxygen-carrying capacity of haemoglobin. It can be measured invasively with an arterial blood sample and noninvasively with an oximeter, which is the standard method for monitoring in anaesthetised patients. The non-invasive method measures the absorption of specific light wavelengths passing through the finger bed and is very accurate for oxygen saturations over 70% [27]. Capnometry, on the other hand, is the measurement of the concentration of carbon dioxide CO₂ in exhaled air. It is a non-invasive method used during intensive care, anaesthesia, and lung function tests. Tidal volume measures the amount of inhaled and exhaled air during a respiratory cycle. Capnometer and tidal volume both use tracheal intubation during measurement. The study on chest wall movement has also been explored based on three similar but

distinctive approach: (i) based on the record of chest wall strain caused by the respiratory activity, (ii) based on the transthoracic impedance change and (iii) based on the record of thorax tridimensional movements (e.g., thorax inclination, acceleration, and velocities) [25].

2.3 Comparison of properties of selected respiratory pressure sensors for MRR

2.3.1 Acoustic pressure sensors

Multiple pieces of research have been done in determining the use of acoustic monitoring technology to monitor the ventilatory rate. Acoustic respiratory rate (RRa) is a non-invasive technology developed as an alternative method for MRR. Acoustic sensors work on a principle based on the sensitivity to physical changes of the environment surrounding the sound source [25]. The most frequent sensor used is the microphone which is a pressure transducer that converts or translates acoustic vibrations into electrical signals recorded in a medium. It is composed of a diaphragm and a displacement transducer which converts the diaphragm's deflection into an electrical signal [28]. From [18], acoustic sensors are practical, and they have a metrological property of high sensitivity which sometimes limits its accuracy due to the interference of movement artefacts and the difficulty in their cancellation.

However, Jafarian et al. [29] developed a six-channel amplification system for perioperative respiratory monitoring on which microphones were attached to the left and right midclavicular, sternal notch, heart, and trachea for the recording of acoustic signals. They concluded that the system would be able to record both in the inspiratory and expiratory circuits sound from the left and right lungs and further proposed that recordings from the heart, trachea, and ventilatory sounds might help recognise clinical conditions such as wheezing, bronchospasm intubation, and apnoea. Ramsey et al. [30] developed a bioacoustics ventilatory rate monitoring device that determines the accuracy and precision of monitoring respiratory rate. They compared the bioacoustic monitors to that of the capnometer, which is a device that monitors the concentration of CO₂ in exhaled air. In conclusion, they stated that bioacoustic monitor was more sensitive in detecting pauses in ventilation hence statistically more accurate than the

capnometer. The MRR using acoustic monitoring devices can be useful and convenient in post-surgical patients [29, 30]. Cashman, J.N., and S.J. Dolin [31] studied the respiratory and hemodynamic effects of acute postoperative pain management. Buhre et al. [20] reviewed perioperative respiratory monitoring in anaesthesia. Its accuracy in paediatric patients has been studied by Patino et al. [32]. It also demonstrates accurate measurement in patients recovering from anaesthesia [33]. The use of acoustic monitoring devices can sometimes be limited due to the interference of sound signals from several other sources such as heart sounds, friction rubs, and the surrounding environment [34]. Kim et al. [35] studied the effect of dental scaling noise during intravenous sedation on the acoustic respiration rate (RRa). They evaluated whether the noise from an ultrasonic scaler affects the performance of RRa during respiratory rate measurement. Data from 49 volunteers who underwent scaling under intravenous sedation was analysed with clinical subjects divided into preparation, sedation, and scaling periods. The rate of respiratory was measured at 2-s intervals for 3 min in each period. They concluded that the probability of missing respiratory rate values was higher during scaling when RRa was used for measurement [35].

2.3.2 Fibre-optic pressure sensors (FOS)

Another technological method for MRR involves the use of FOS. FOS uses optical fibre or sensing elements which are distinguished by their core size for detecting mechanical strains and some quantities such as pressure, temperature, vibration displacements. Due to its unique insensitivity to electromagnetic fields makes optical fibres a popular tool for biomedical devices [36]. Its insensitivity to electromagnetic field happens to be of great importance, especially in the hospital environment where there have been reports of electromagnetic interference (EMI) with electronic medical equipment [37]. [25] reviewed the use of FOS in several contact-based techniques for MRR, as shown in Figure 5. Krehel et al. [38] in a 2014 publication, presented a textile-based respiratory sensing system. They created a wearable sensing system by attaching highly flexible polymeric optical fibres (POFs) that react to the application of pressure. With the attachment of the wearable sensors to different positions on the torso, it was possible to record measurements of respiratory rate. They concluded that depending on the way of breathing, the signal amplitude was different for each position on the

torso where the FOS are placed, and the integration of two or more sensors allows not only the recording of breathing rate but also the way of breathing [38]. [39] proposed the use of intensity-based FOS to help distinguish breathing conditions. Fibre Bragg grating (FBG) [40] sensors are another type of FOS used in MRI procedure that has also been studied which involves placing the sensors in the nasal-cavity for the monitoring of respiratory frequency and signals.

2.3.3 Resistive pressure sensors

Resistive sensors are sensors or resistors that detect changes in resistance due to environmental influences such as pressure, light, temperature, strain, etc. Resistance [R] with SI unit in ohms (Ω) is an electrical quantity that measures the rate of change in electric current through a material or device, and it depends primarily on the shape and composition of the material.

$$R = \frac{\rho l}{A} \quad (2)$$

Eq 2 describes the resistance of a material, where A is the Cross-sectional area (m^2), ρ is electrical resistivity ($\Omega.m$), and l is material length (m). Resistive sensors such as thermistors, strain gauges, potentiometer, are known for their high sensitivity property. This makes it convenient and practical for application into biomedicine and other clinical studies. Techniques based on relative humidity use resistive sensors in the application of monitoring respiratory frequency, and it works [25] with a principle based on the electrical impedance change in humidity. Relative humidity sensors monitor respiratory frequencies by detecting the difference in water vapour content between inspiratory and expiratory air.

Furthermore, [25] reviewed the use of piezo-resistive strain sensors that functions as a result of the changes in electrical charge concentration caused by an external strain with techniques based on chest wall movement. With techniques involving chest wall movement, resistive flexible sensors can detect slight changes in chest and abdominal

movement during breathing. Textile sensors were used in another study to detect talk events based on changes in breathing pattern [41].

2.3.4 Capacitive pressure sensors

Capacitive sensors, otherwise, biosensors are types of biosensors categorised into pressure or impedance sensors [42]. This type of sensors measures the changes in dielectric properties and or thickness of the dielectric layer at the electrolyte/electrode interface [43]. A capacitor in its basic form consists of two or more parallelly conductive metal plates electrodes that are not directly connected but are electrically separated by an insulating material or air. The insulating surface separating the parallel conductive metal plates is commonly called **dielectric**. Through the formation of the insulating surface, we can measure the electric capacitance C , (Farads) using to Eq 3:

$$C = \epsilon_0 \epsilon_r \frac{A}{d}, \quad (3)$$

where ϵ_r is the relative permittivity, ϵ_0 is the permittivity of the free space (8.85×10^{-12} F/m), A denotes the surface area of the plates (m^2), and d is the thickness of the insulating layer (m). Capacitive sensors can be used in the monitoring of respiratory frequencies in techniques such as relative humidity and chest wall movement [25]. In one instance, researchers have developed a respiratory sensor belt by using electrochemical film EMFit, which is a type of capacitive pressure sensor [44] for measuring respiratory rate. Capacitive sensors have also been successfully used for the detection of proteins, nucleotides, heavy metals, saccharides, small organic molecules, and microbial cells [43]. High capacitance means small impedance [45].

2.3.5 Schematic comparison

Sensors are devices that receive or respond to stimuli and signals. [46] distinguishes sensors into three types;

- I. Physical sensors for measuring physical quantities (temperature, pressure, etc.)
- II. Chemical sensors that respond to chemical changes,
- III. Biosensors that monitor chemical changes using biological sensing elements.

To best explain the comparison of the selected respiratory pressure sensors described above, it is essential to understand the properties of sensors and specific terminologies that can best describe its specifications and provide details on its ability to react and detect the changes in physical quantity.

RANGE: The range of a sensor is the maximum and minimum value range over which an applied parameter can be measured. [47] for example, a particular medical blood pressure transducer is specified to have a minimum (vacuum) limit of -50 mmHg and a maximum (pressure) limit of +450 mmHg. Operating sensors outside its given range may lead to malfunction. However, it can be used when additional calibration is done.

SENSITIVITY: It is the minimum input value of a physical parameter that can provide a detectable change in output. In other words, it is an output change in voltage due to a change in the given input parameter. For instance, [47] a typical blood pressure transducer may have a sensitivity rating of 10 mV/mmHg; i.e., there will be a 10mV output voltage for each volt of excitation potential and mmHg of applied pressure.

The value determined from the best-fit straight line represents a sensitivity averaged for the calibrated range.

F = Reference signal (force) [N]

Q = Generated signal (charge) [pC]

S = Sensitivity $\frac{\Delta Q}{\Delta F}$ [pC/N]

PRECISION: The precision refers to the degree of reproducibility of measurement [47]. It accounts for a sensor's ability to reproduce the same output value every time a given measurement is done or its ability to repeat a measurement when put back in the same physical condition. It is often related to the accuracy of a sensor. It is important to note that sensors can sometimes be inaccurate but repeatable

ACCURACY: is defined as the maximum difference between the actual value and the sensor output- a higher accuracy results in lower the error, represented in percentage error.

OUTPUT LINEARITY: Linearity accounts for the extent to which the actual output curve of the sensor deviates from the ideal curve, and is expressed in terms of percentage of non-linearity. Linearity describes the consistency of measurement over an entire range of measurements. Dynamic linearity describes the ability of the sensor to follow a rapid change in input.

RESPONSE TIME: is defined as the time required for a sensor output to change from its previous state to a final settled value within a tolerance band of the correct new value [47].

There is a broad spectrum of intelligent sensors that have been studied and experimented with to create alternative and cost-effective ways for MRR. Each of these sensors possesses distinguishable and unique property, hence function using different principles.

Acoustic sensors are susceptible to interference of both background noise and activity from the subject not related to breathing. Such interference affects the accuracy in measurement and may require further signal processing in their cancellation. Based on the metrological properties [25], acoustic sensors have good sensitivity and response time. However, their accuracy is mostly questioned; hence, they are usually not recommended for use in clinical settings. On the other hand, FOS potentially has several advantages [25] (small size, short response time, usability in harsh environments). They also have high sensitivity and have been used in various techniques for MRR such as air humidity, air temperature, chest wall movement, etc.

In the case of resistive sensors, they have shown excellent performance up to very high respiratory frequency values (e.g., up to 240 bpm), especially in techniques based on air humidity [48]. They are quite sensitive and show good response time [25]. Their use as strain sensors in the form of *piezo-resistive* sensors for monitoring deformation of chest wall movement shows that the sensor output may be affected by motion artefacts and has poor durability. However, piezo-resistive sensors have been experimentally integrated into an automobile safety belt to monitor respiration [8]. With capacitive sensors, their sensitivity relies on electrodes number, size, the distance between them, and the position of the electrodes [49]. According to [49], they concluded from their study that their designed capacitive sensor showed accurate measurement and recommended its use in clinical settings.

Different other types of pressure sensors were not included in this study. However, their application into several industries and technology systems have progressively been studied and explored as alternatives to other sensor types. Pressure sensors can be used in different medical devices such as spirometry devices for lung capacity testing, ventilators for monitoring oxygen pressure, treatment process in a hyperbaric chamber, transducer, and many more.

3. PIEZOELECTRIC SMART MATERIALS

3.1 Characterisation of relaxor based materials

3.1.1 Overview of typical ferroelectrics and relaxor ferroelectrics

The ferroelectric phenomenon was first discovered in a single crystal of sodium-potassium tetratetrahydrate ($\text{NaKC}_4\text{H}_4 \cdot \text{H}_2\text{O}$), also known as Rochelle salt [50]. Since its conception, many other ferroelectric ceramics have been discovered such as lead zirconate titanate $\text{Pb}(\text{Ti}, \text{Zr})\text{O}_3$ (PZT), lead titanate (PbTiO_3), lead lanthanum zirconate titanate (PLZT), LiNbO_3 , KNbO_3 , LiTaO_3 , $\text{Pb}(\text{ZnNb})\text{O}_3$. However, it was not until the discovery of barium titanate (BaTiO_3) in the 1940s that it led to extensive research in ferroelectricity and saw its expansion into the engineering industry [51]. BaTiO_3 possess different polymorphic forms and is the most important of the perovskite family of ferroelectric. It has an excellent dielectric and ferroelectric properties [52], with a Curie temperature T_c of 120 °C, and synthetic techniques in yielding nanocrystals [52, 53], but is not an ideal piezoelectric material for device applications because of its relatively poor temperature stability [54]. Ferroelectric materials are characterised by high dielectric constant, spontaneous polarisation, and presence of pre-existing dipoles even in the absence of an applied electric field. It is an electrical analogue of ferromagnetic materials. Their properties make them applicable to be used in ferroelectric memories, high permittivity capacitors, piezoelectric transducers, electrooptic devices [55].

Spontaneous polarisation is caused by a distortion in the crystallographic structure, resulting in a dipole moment and separation of charges within the crystal. The constituent atoms within the crystals are ionised through electrostatic attraction by the application of an external electrical field, hence creating electric polarisation. Polarisation can be expressed quantitatively as the sum of electric dipoles per unit volume [C/m^2]. Spontaneous polarisation changes with temperature, which is usually determined by the *Curie temperature* T_c . T_c defines the transition from an electrically neutral state to spontaneous polarisation, thereby, differentiating one crystallographic phase from another. Temperatures of crystals above the T_c are electrically neutral and

possess a *paraelectric* crystallographic phase while crystal below the T_c shows spontaneous polarisation with a crystallographic phase known as *ferroelectric* [44].

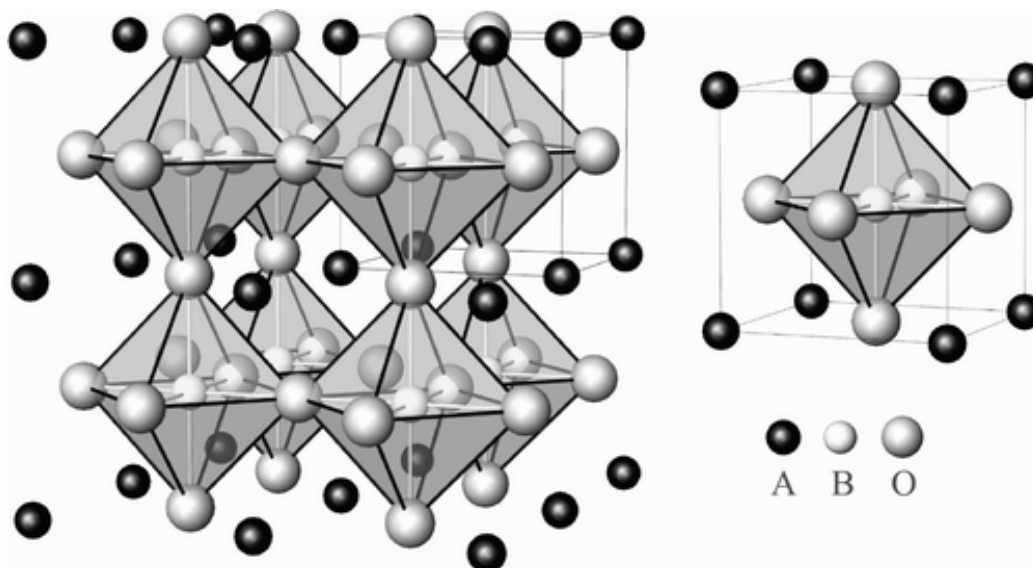
Lead containing perovskites (ABO_3), called relaxor such as Lead magnesium niobite ($PbMg_{1/3}Nb_{2/3}O_3$) PMN, and lead zinc niobite ($PbZn_{1/3}Nb_{2/3}O_3$) PZN are characterised by a strong frequency dispersion of the permittivity [45, 55]. Scientists have extensively been studying perovskite materials over the years, and they found out that they exhibit very high permittivity over a wide range of temperatures, intense electrooptic activity (which is the change in refractive index with an external electric field), strong piezoelectric and pyroelectric effect, [55]. However, they depend on a strong temperature to obtain strain. The dielectric susceptibility of relaxors have a broader peak above the curie temperature unlike conventional ferroelectrics that possesses a sharp peak, and below this temperature, most relaxor remains cubic showing no electric polarisation as compared to that observed in conventional ferroelectrics [56]. The relaxor behaviour is due to the presence of polar nanoscale domains/regions (PNR), which vary in temperature.

Lead magnesium niobite (PMN) is one of the most interesting relaxor ferroelectric materials. It has a randomly disordered complex structure in which the Mg^{2+} and Nb^{5+} cations exhibit a short-range order on the B-site and together with other perovskite have a cubic symmetry at room temperature [56] as shown in figure 6. $BaTiO_3$ is cubic above 135 °C but transforms into a tetragonal ferroelectric structure below this temperature [57]. $PbTiO_3$ has a single transition to tetragonal phase at 490 °C while some other perovskites show structural phase transition that is not ferroelectric as shown in Table 2. Table 2 shows a list of phase transition at room temperature and Curie temperature formed by some perovskite compounds along with their tolerance factor. The tolerance factor is a predictor of the stability of perovskite compounds possess, notably the Goldschmidt tolerance factor.

Table 1: Some perovskite and their properties [57]

Perovskite oxide	Tolerance factor	Structure at 20 °C	Type	Curie Temperature T_c (°C)
BaTiO ₃	1.06	Tetragonal	Ferroelectric	135
SrTiO ₃	1.00	Cubic	Paraelectric	
CaTiO ₃	0.97	Tetragonal	Paraelectric	
PbTiO ₃	1.02	Tetragonal	Ferroelectric	490
PbZrO ₃	0.96	Orthogonal	Antiferroelectric	235
NaNbO ₃	0.94	Monoclinic	Ferroelectric	-200
KNbO ₃	1.04	Tetragonal	Ferroelectric	412
KTaO ₃	1.02	Cubic	Ferroelectric	-260
BiScO ₃	0.83	Rhombohedral	Ferroelectric	370
BiFeO ₃	0.87	Tetragonal	Ferroelectric	850

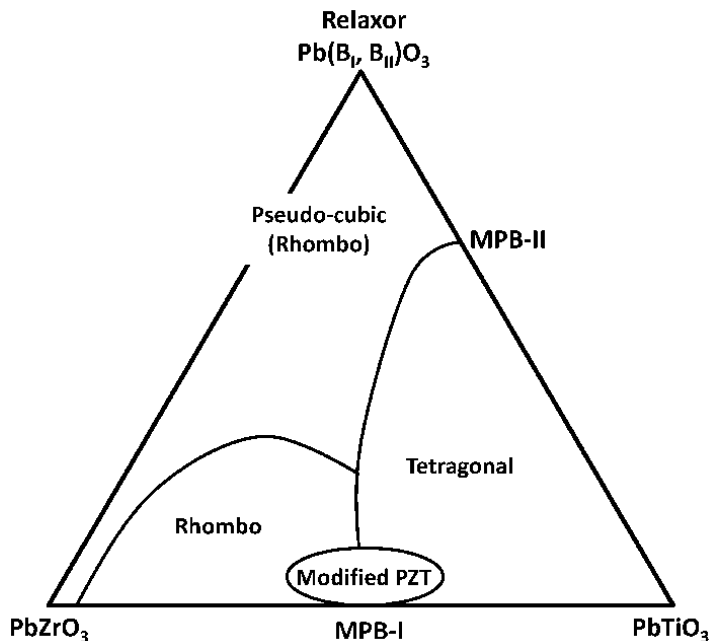
Figure 6: The ideal cubic perovskite structure. Large open circles denote the oxygen atoms, smaller open and solid circles denote the metal cations with A and B sites, respectively. [56]



3.1.2 Morphotropic phase boundary (MPB) and Domain structure of ceramic materials

Some solid perovskite solution type ferroelectrics show properties that lie along the morphotropic phase boundary (MPB). The MPB is an abrupt structural phase transition between the cubic, tetragonal, rhombohedral, monoclinic (orthorhombic, or triclinic) phase. The mechanical and electrical properties of ferroelectrics materials are usually enhanced by the MPB [58, 45, 55] which separates one structural phase from the other. Near the MPB composition, the structure is relatively less stable, which produces more significant responses under external stimuli, temperature, electric field, and stress [54]. The MPB of PZT ceramics lies between the tetragonal and rhombohedral phase as depicted in Figure 7, and anomalously exhibit high dielectric and polarisation properties resulting from the coupling between two equivalent energy states that allows for domain orientation for pooling process [59, 60]. They have a paraelectric cubic phase above their Curie temperature, and its ferroelectric phase divided into two regions with different crystal symmetries [54]. Figure 7 shows a phase diagram of the MPB exhibited by PZT and relaxor materials.

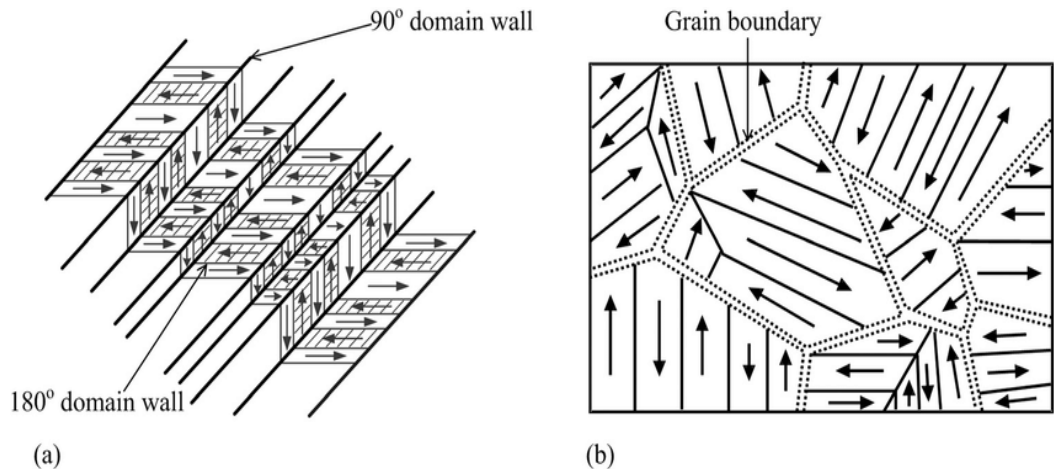
Figure 7: Tertiary phase diagram depicting MPBs in PZT and Relaxor-PT system in piezoelectric ceramics [59]



The MPB of the $(1-x)\text{Pb}(\text{Mg}_{1/3}\text{Nb}_{2/3})\text{O}_3-x\text{PbTiO}_3$ (PMN-PT) system is located close to the $x=0.35$ composition [61] whilst $\text{Pb}(\text{Zn}_{1/3}\text{Nb}_{2/3})\text{O}_3-x\text{PbTiO}_3$ (PZN- x PT) system is between $x = 0.09 - 0.11$ [62]. PZN-PT is a solid solution of relaxor ferroelectric and has a rhombohedral to tetragonal MPB to that of PZT.

The individual dipoles in ferroelectric ceramics are arranged in a particular order called *domains*. Domains are separated by *domain walls* which can lie in planes of $\{100\}$ for 180° walls since they separate domains at 180° and $\{110\}$ for 90° walls for separating domains inclined at 90° [45], and other domains are $\{001\}$ for 71° , 90° [63, 45]. Dipoles within the domain have a *parallel orientation* or are oriented in the direction of the domain walls, as shown in Figure 8. The orientation of dipole between domains is *random*, and at zero field, there is no net polarisation due to the random orientation between domains. When an electric field is applied, there is a change in dipole orientation. The polarisation directions of ferroelectric domains can be switched by a sizeable electric field or by high stress if the material is also ferroelastic, which is called domain switching [64]. Domain switching is an irreversible and energy dissipation process [65, 64]. Domain boundary movement can lead to hysteresis. Figure 8a describes the angle of orientation by the domain walls, while figure 8b shows the boundaries separating one domain form another.

Figure 8: Schematic depiction of a typical domain structure [64]



3.1.3 Relaxor-based Ferroelectrics and its properties

Relaxor-based ferroelectrics are solid solutions of relaxors and PbTiO_3 represented as "relaxor-PT". They possess both properties of relaxor ferroelectrics (PMN, PZN) and normal ferroelectrics (PT). They are lead-based perovskite compounds with formula $\text{Pb}(\text{B}_I\text{B}_{II})\text{O}_3$, where B_I represents a divalent/trivalent element, E.g. (Mg^{2+} , Zn^{2+} , Ni^{2+} , Fe^{3+} , Sc^{2+} , etc.) and B_{II} , E.g. (Ti^{4+} , Nb^{5+} , Ta^{5+} , W^{6+} , etc.) [57, 54]. Furthermore, they are classified as B-site perovskite based on their crystal structure and composition. The commonly used single crystals relaxor-PT are $(1-x)\text{Pb}(\text{Mg}_{1/3}\text{Nb}_{2/3})\text{O}_3-x\text{PbTiO}_3$ (PMN-PT), $(1-x)\text{Pb}(\text{Zn}_{1/3}\text{Nb}_{2/3})\text{O}_3-x\text{PbTiO}_3$ (PZN-PT) and $(1-x-y)\text{Pb}(\text{In}_{1/2}\text{Nb}_{1/2})\text{O}_3-y\text{Pb}(\text{Mg}_{1/3}\text{Nb}_{2/3})\text{O}_3-x\text{PbTiO}_3$ (PIN-PMN-PT) and their remarkable properties have led to the fast commercialisation into high-end ultrasonic imaging in the medical field and are now used to replace the traditional PZT piezoceramic that has been used mainly in high-performance actuator applications. Relaxor-based materials are characterised by ultra-high electromechanical coupling factor $k_{33} > 90\%$, with their composition near the morphotropic phase boundary (MPB) along with possessing low dielectric loss ($< 1\%$) and piezoelectric properties [54, 45]. The characterisation of relaxor-PT is based on their electromechanical coupling (k_{ij}), high piezoelectric coefficient (d_{ijk}), high dielectric constant (ϵ), and elastic properties. These properties are discussed considering strain, electric field behaviour, polarisation, domain stability, and their response to temperature.

3.1.1.1 Piezoelectric and Electromechanical coupling factor properties

The term piezoelectricity comes from the *Greek* root "*Piezen*" meaning "*to press*" and *Latin* root "*electrum*" meaning "*amber*". Piezoelectricity which is usually represented as the piezoelectric coefficient (d_{ijk}) is a property of ceramic materials (quartz crystals and lead-based ceramics) to develop electrical displacement D_i on its surface when mechanical stress T_λ (pressure or bending) is applied to it, i.e., the ability of piezoelectric materials to convert mechanical energy into electrical energy (direct piezoelectric effect) and vice versa. Upon the application of an electric field E_j , piezoelectric material deforms resulting in a converse piezoelectric effect. These can be mathematically represented in tensor notation as,

$$P_i = d_{ijk}\sigma_{jk} \text{ (direct effect)} \quad (4)$$

$$\epsilon_{ij} = d_{kij}E_k \text{ (converse effect)}, \quad (5)$$

Where P_i represents polarisation generated along the i -axis with an applied stress σ_{jk} , and d_{kij} is the piezoelectric coefficient. The converse effect, ϵ_{ij} is the strain generated in a particular orientation of the crystal when an electric field E_k applied along the k -axis. Electric field behaviour is usually expressed by following the stain level. These two parameters determine the domains (in) stability and electric field behaviour can further express hysteresis from dipole polarisation. Hysteresis is formed as a result of saturation in polarisation when all the domain walls become parallel to the direction of applied E-field. An applied electric field (E) tends to align elementary dipole moments in a particular direction. However, complete alignment can only be obtained practically with a very large electric field E exceeding the breakdown field of the material [66].

The electromechanical coupling factor (k_{ij}), is an indicator of the effectiveness with which a piezoelectric material converts electrical energy into mechanical energy, or converts mechanical energy into electrical energy [67]. The coupling factor is determined by the square root of the ratio of stored mechanical energy to the total energy absorbed and vice versa. If mechanical energy act as input on the piezoelectric material, electromechanical coupling factor k (strictly speaking k^2) will result from Eq: 6 [68]

$$k^2 = \frac{\text{mechanical energy converted into electrical energy}}{\text{input mechanical energy}} \quad (6)$$

And in the case of input energy from Eq: 7

$$k^2 = \frac{\text{electrical energy converted into electrical energy}}{\text{input electrical energy}} \quad (7)$$

Even though relaxor-PT possesses unique characteristics, but its exceptionally high piezoelectric property made it a more desirable component for electromechanical devices. Currently, PZT polycrystalline ceramics are used with piezoelectric coefficients (d_{33}) ranging from 200 to 750 pC/N, with the later limited by hysteresis while electrostrictive ceramics such as PMN offers effective d_{33} 's >700 pC/N, and piezoelectric d_{33} value as high as ~ 2000 pC/N found for MPB composition in both

PMN-PT and PZN-PT systems [45, 59]. The large piezoelectric constant ($d_{33} > 2500$ pC/N) of $[001]_c$ poled rhombohedral single crystals is five times that of the best modified PZT ceramics ($d_{33} \sim 500$ pC/N). The subscript "c" indicates that the crystallographic orientation refers to the cubic crystal structure. The electromechanical coupling factor k_{33} is more than 90%, and the dielectric loss is less than 1% [54]. PMN-PT and PZN-PT single crystals have a super large piezoelectric coefficient, electromechanical coupling factors and can be grown relatively quickly, but they also have some disadvantages, such as low thermal stability (low rhombohedral to the tetragonal phase transition temperature, $T_{RT} \sim 50\text{--}75$ °C) and relatively low Curie temperature ($T_c \sim 150\text{--}170$ °C), which restrict them from some applications that require better thermal stability [54]. For these materials to achieve a high piezoelectric coefficient, their MPB-based ceramics are further engineered by compositionally adjusting the Curie temperature T_c downward relative to room temperature. Table 3 shows piezoelectric coefficients and electromechanically coupling factors for different materials.

Table 2 Comparison of piezoelectric constants and electromechanical coupling factors of conventional piezoelectric and ferroelectric materials. [54]

Materials	Point group symmetry	Piezoelectric constants	Electromechanical coupling factor
Alpha-quartz crystal	32	$d_{11} = 2.31$ pC/N $d_{14} = 0.727$ pC/N	$k_{11} = 10\%$
BaTiO ₃ ceramic	6mm	$d_{31} = -79$ pC/N $d_{33} = 191$ pC/N	$k_{31} = 21\%$, $k_{33} = 50\%$
BaTiO ₃ single crystal	4mm	$d_{31} = -32.5$ pC/N $d_{33} = 90$ pC/N	$k_{31} = 32\%$, $k_{33} = 55\%$
LiNbO ₃ single crystal	3m	$d_{31} = -0.85$ pC/N $d_{33} = 6$ pC/N	$k_{31} = 2\%$, $k_{33} = 17\%$
LiTaO ₃ single crystal	3m	$d_{31} = -3$ pC/N $d_{33} = 5.7$ pC/n	$k_{31} = 7\%$, $k_{33} = 14\%$
Pb(Zr _{0.52} Ti _{0.48})O ₃ ceramic	6mm	$d_{31} = -93.5$ pC/N $d_{33} = 223$ pC/N	$k_{31} = 31\%$, $k_{33} = 67\%$
[001] _c poled PMN-33%PT single crystal	4mm	$d_{31} = -1330$ pC/N $d_{33} = 2820$ pC/N	$k_{31} = 59\%$, $k_{33} = 94\%$
[001] _c poled PZN-8%PT single crystal	4mm	$d_{31} = 1455$ pC/N $d_{33} = 2890$ pC/N	$k_{31} = 60\%$, $k_{33} = 94\%$

The piezoelectric performance and electromechanical coupling factor of relaxor-PT are relatively dependent on the type of crystalline growth. In its polycrystalline state, Relaxor-PT does not offer significant piezoelectric performance compared to PZT ceramics, but in their single crystalline form offer significant enhancement with electrochemical coupling factor greater than 90% with electric field exceeding 1% in contrast to ~ 75% and 0.1% levels in polycrystalline PZT ceramics [45]. The growth of crystals can be done using high-temperature flux growth or Bridgman growth.

3.1.1.2 Dielectric and elastic properties

Relaxor-PT materials have demonstrated a superior dielectric property as compared to conventional ferroelectrics. Normal ferroelectrics (BaTiO_3 and PbTiO_3) have a sharp dielectric peak that is independent of frequency. Unlike normal ferroelectrics, relaxor-PT are characterised by a broad peak and a dielectric maxima frequency dispersion. At higher temperatures and increased frequency, the dielectric constant decreases causing a dielectric loss. Broad dielectric response with temperature and strong dielectric relaxation with frequency has long been attributed to the formation of polar nanoregions (PNRs), in a non-polar matrix where the Burns temperature (T_b) and maximum dielectric temperature (T_m) is thought to be related to the formation and onset of the slowing-down of the dynamics of the PNRs [69]. The elastic and dielectric performance of electromechanical devices is temperature dependent. A high permittivity is associated usually with an increase in dielectric losses [70]. Sabat et al., [71] studied the temperature dependence of the dielectric, elastic, and piezoelectric constants of soft and hard doped PZTs and concluded that dielectric permittivity coefficients ϵ_{11}^T , and ϵ_{33}^T , generally increased with temperature for both soft and hard PZT samples. However, the elastic compliance coefficients s_{11}^E , $-s_{12}^E$, s_{33}^E and s_{55}^E exhibited abnormal variations seen as broad peaks over parts of the tested temperature range. Liguio et al. reports using the resonant ultrasound spectroscopy (RUS) technique to characterise the temperature dependence of full tensor material constants of a $[001]_c$ poled Mn-doped 0.24PIN-0.46PMN-0.30PT single crystal from 25 - 55 °C [72].

3.2 Conceptual design of the sensor

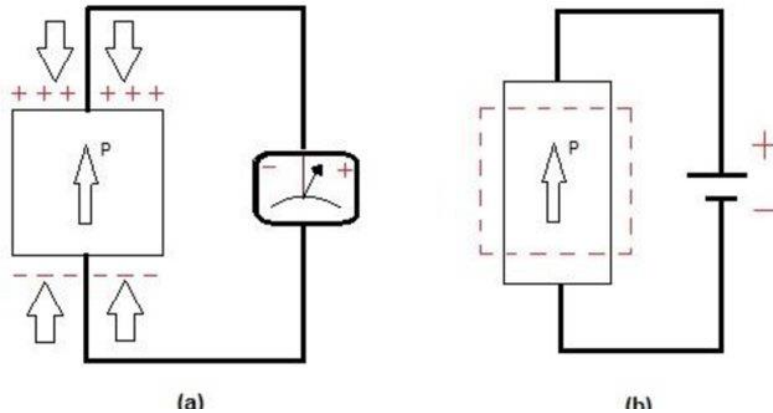
Smart materials, otherwise intelligent materials, mostly sensors and actuators are materials with a substantive response to external stimuli of electrical, mechanical, magnetic, or chemical by changing its shape or form. This exceptional sensing ability makes these materials very desirable for electromechanical devices and has revolutionised the entire technology industry. We can see its impact across all spheres ranging from automobile, electronics, medical industry, and many more. Some smart materials have a memory shape ability that enables them to return to their original

shape and size after induced external stimuli. Shape-memory alloys [73] which are a sub-group of smart materials return to their pre-deformed shape, and this structural change is due to the reversible crystalline structure within them. Alloys (Cu-Al-Ni, Ni-Ti-Cu, Ti-Pd-Ni) change their crystal structure and shape above the phase transition temperature θ_{TR} [74]. Nitinol, a memory shaped alloy, has been engineered for orthopaedic implants; it contracts when heated and returns to its original size and shape when cooled.

3.2.1 Piezoelectric sensor

The conceptual design of the sensor used in this thesis comes from the principle of energy conversion. A piezoelectric ceramic sensor is the desired materials, and it obeys the principle of energy conversion by converting mechanical energy created from stress or pressure to electrical energy and vice versa. Piezoelectric sensors use the piezoelectric effect, which results from the linear electromechanical interaction between the mechanical and electrical states [75]. The piezoelectric effect makes it possible for this reversible transformation to occur and can happen in two ways, either as a direct piezoelectric effect or inverse/converse piezoelectric effect. Direct piezoelectric effect Figure (9a) occurs when a material generates electrical charge Q otherwise piezoelectricity from the direct application of a force, mechanical stress, or pressure. Examples of some devices that use the direct piezoelectric effect include pressure sensors, microphones, hydrophones, etc. On the other hand, the application of electrical voltage/field to a piezoelectric plate, which results in its shrinking and expansion causes converse/inverse piezoelectric effect Figure (9b). The inverse piezoelectric effect can create acoustic sound waves similar to other acoustic devices like speakers, ultrasound transducers, and sonar transducer. By applying an electrical AC/voltage of the frequency, f_0 produces the ultrasonic wave in transducers. The inverse piezoelectric effect can also produce non-acoustic sound waves found in motors and actuators.

Figure 9: Direct and converse piezoelectric effect [76]



The resulting electrical charge that forms on the surface of some crystal materials and ceramics by an applied mechanical force is known as piezoelectricity. Piezoelectricity is the property of all materials that have a non-centrosymmetric crystal structure, typically all polar materials except for quartz (SiO_2) which is non-polar and piezoelectric but not pyroelectric [70]. The centrosymmetric crystals such as cubic crystals of the silicon Si are not piezoelectric [74]. Piezoelectric material exists as a single crystal (quartz, LiNbO_3 , LiTiO_3), thin-film (AlN , ZnO), polymer (PVDF), and ceramic (BT, PZT). Using quartz crystals as an example, we can explain how the crystallographic structure of these materials enables the production of piezoelectricity.

3.2.2 Structural arrangement in a piezoelectric quartz crystal

Quartz crystal has a chemical composition of silicon oxide (SiO_2) which is a single unit and exists in two forms, the normal α -quartz and the high-temperature β -quartz [77], with a structural phase transition at $573\text{ }^\circ\text{C}$ [70]. They possess excellent electromechanical properties which makes it suitable for different devices. Quartz crystal has a hexagonal/trigonal system with the crystal plate having a trigonal axis and diagonal axes, which are at right angles to the trigonal axis. The general arrangement of the atoms and electrons in an α -quartz crystal is such that each Si atom is tetrahedrally surrounded by four pairs of O_2 atoms, as shown in Figure 10. However, viewing it from the z -axis gives a proper depiction of the trigonal system in a single

unit of quartz crystal, Figure 11. The orientation of the plate is in the x, y, and z plane of which the x-axis (electric axis), y-axis (mechanical axis), and z-axis (optical axis) Figure 12. The X-axis and Y-axis are the two-fold symmetry axis and each pair of $X_1 - Y_1$, $X_2 - Y_2$, and $X_3 - Y_3$ axes have the same characteristics and relationships to each other Figure 13 [78].

Figure 10: shows the unit cell of α -quartz. Small black circles show the Si atom and the large white circles show the O atom [78]

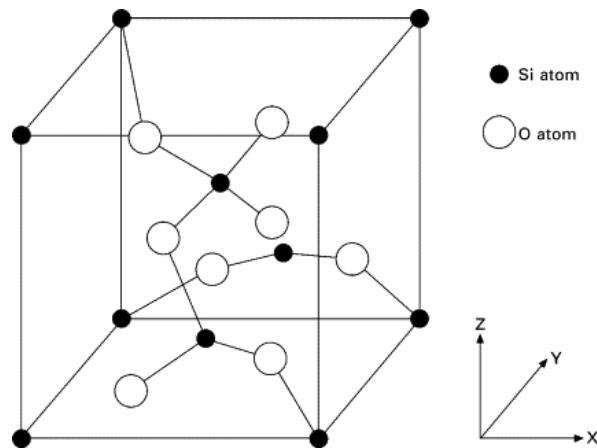


Figure 11: Single unit of Si and O atoms viewed from the Z-axis [78]

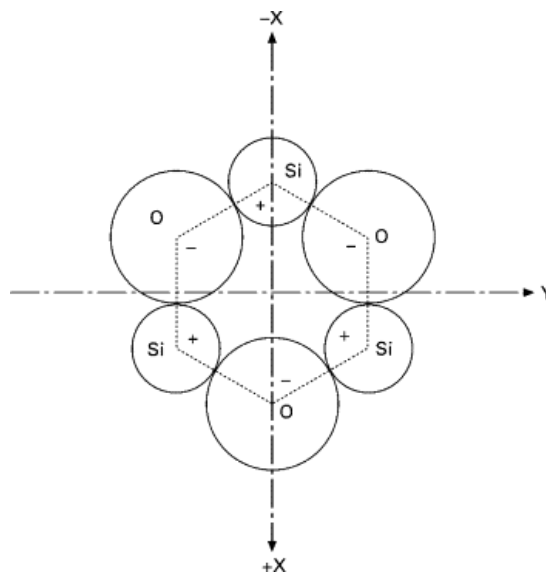


Figure 12: Quartz crystal plate x, y, z plan [78]

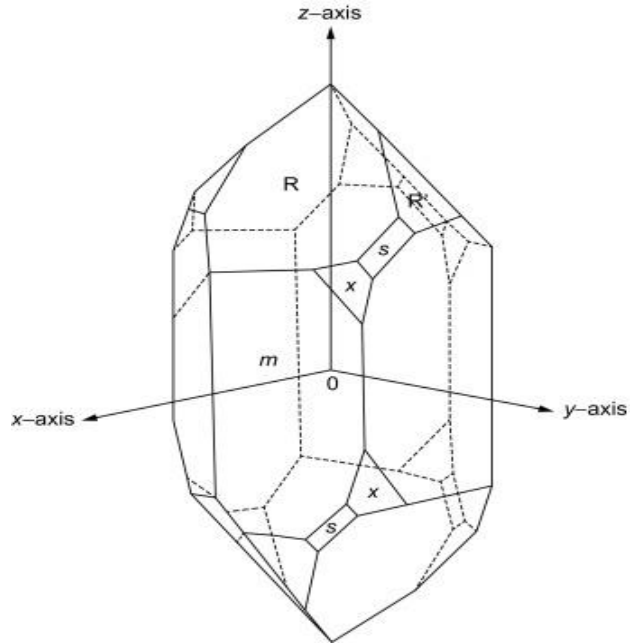
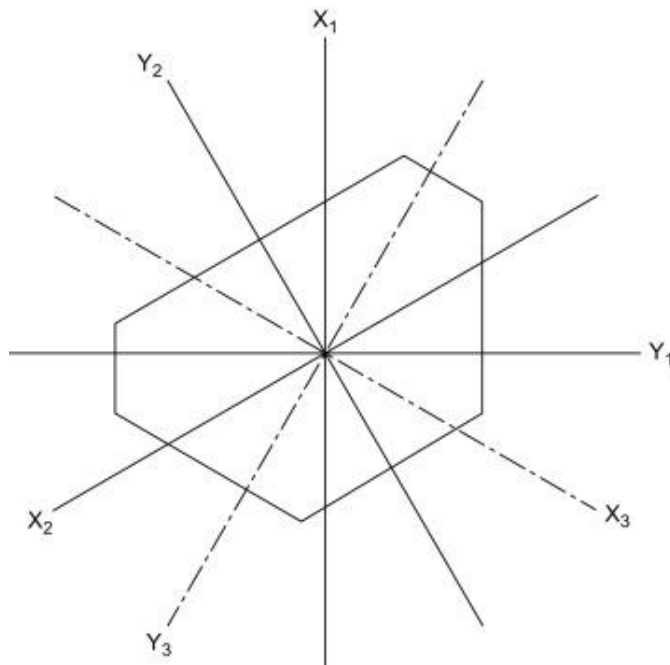


Figure 13: X-axis (electric axis) and Y-axis (mechanical axis) are the two-fold symmetry axis [78].



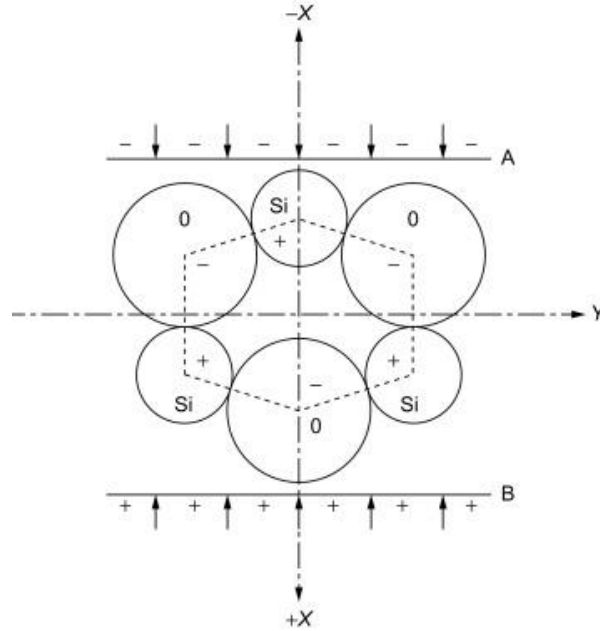
Depending on the type of designed sensor, different mechanisms can be used in creating a piezoelectric effect in quartz crystal. The piezoelectric effect could be distinguished based on the direction displacement from the applied Force field, which occurs in 3 directions.

1. Longitudinal effect
2. Transversal effect
3. Shear effect

3.2.1.1 Longitudinal effect

The longitudinal piezoelectric effect is created from compressing or applying mechanical Force along the x-axis of the crystal plate, causing the three electrically centred Si and O atoms to distort and create polarisation along the x-axis. Figure 14 shows the mechanism of the longitudinal piezoelectric effect. When the crystal plate is compressed along the x-axis, the externally charged Si and O electrons will move outwards. This will cause in the top Si and bottom O atoms to move inwards, resulting in the net downwards movement in the positively charged Si and upward movement in the negatively charged O atoms. This net movement will lead to a shift in all the positive charges to one direction and the negative charges to the other direction, causing polarisation. The reverse polarisation will happen when pulling stress is applied to the crystal plate. However, if electrodes are attached on both ends of the plate with an AC electric field applied between them, the mechanical vibration created within the crystal will cause displacement along the x-axis. Coefficient $d_{1\lambda}$, i.e., d_{11} , d_{22} , and d_{33} describes the longitudinal piezoelectric effect [79].

Figure 14: Longitudinal piezoelectric effect [78]



The amount of charge Q produced is strictly proportional to the applied force and is independent of the size and shape of the piezoelectric element. The resulting output charge Q can be derived by using several electrical and mechanical elements, as shown in Eq. 8.

$$Q_x = d_{xx} F_x n , \quad (8)$$

Where d_{xx} is the piezoelectric coefficient for a charge in the x -direction released by force applied along the x -direction (in pC/N). F_x [N] is the applied Force in the x -direction and n correspond to the number of stacked elements.

The charge Q in a quartz plate can be determined,

The Force F_x produces a mechanical stress $\sigma_1 = \frac{F_x}{A}$, where $A = lb$ is the surface area on which F_x is applied.

The charge density q_1 on the electrodes $q_1 = d_{11} \sigma_1$

Total charge $Q_1 = A \cdot q_1 = A \cdot d_{11} \frac{F_x}{A} = d_{11} F_x$ [C] (9)

3.2.1.2 Transverse effect

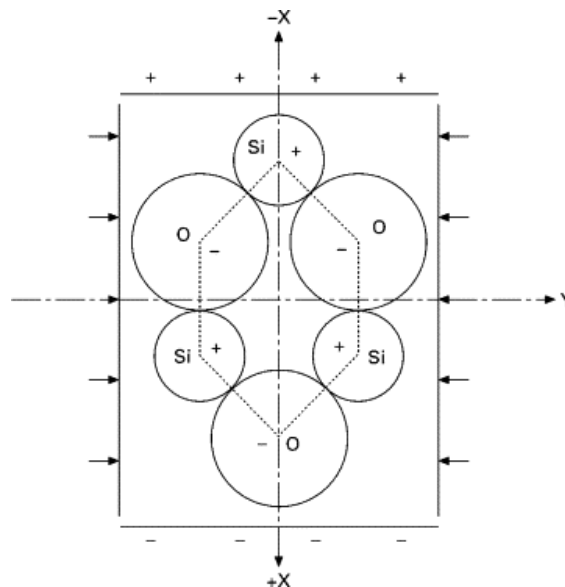
Transverse piezoelectric effect, as shown in Figure 15, results from applying mechanical Force along the y-axis will create polarisation in the direction of the x-axis. There will be an average upward movement in the positively charged Si and downward movement in the negatively charged O. The same result will be yield when an AC field is applied to it.

A force is applied along a neutral axis (y) and the charges are generated along the (x) direction, perpendicular to the line of Force. The amount of charge depends on the geometrical dimensions of the corresponding piezoelectric element. When dimensions a, b, c is applied, the charge will be Eq. (10).

$$Q_x = d_{xy} F_y \frac{b}{a} \quad (10)$$

where a is the dimension in line with the neutral axis, b is in line with the charge generating axis and d_{xy} represents the corresponding piezoelectric coefficient;

Figure 15: Transverse piezoelectric effect [78]



The charge in a quartz crystal can be determined using,

The Force F_y produces a mechanical stress $\sigma_2 = \frac{F_y}{b.a}$, where ba is the surface area on which F_y is applied.

The charge density q_1 on the electrodes $q_1 = -d_2\sigma_2 = -d_{11}\sigma_2$

$$\begin{array}{l} \text{Total} \\ \text{charge} \end{array} \quad Q_1 = l.b.q_1 = l.b.-d_{11}\sigma_2 = -d_{11} \cdot \frac{l}{a} \cdot F_y \text{ [C]} \quad (11)$$

3.2.1.3 Shear effect

The application of shear mechanical stress may result in the possibility of piezoelectric polarisation either perpendicularly or parallel to the plane of applied shear. Shear piezoelectric effect occurring in the perpendicularly plane is called longitudinal shear. It is characterised by one of the following piezoelectric coefficient d_{14} , d_{25} or d_{36} while polarisation occurring parallel is called transverse shear related to one of the following piezoelectric coefficient $d_{1\lambda}$, i.e. d_{15} , d_{16} , d_{24} , d_{26} , d_{34} , and d_{35} [79].

When creating piezoelectricity by shear effect, the electric field in the ceramic layer is applied orthogonally to the direction of polarisation, and the displacement in the direction of polarisation is utilised [80]. For n number of elements mechanically in series and electrically in parallel, the charge is Eq (12).

$$Q_x = 2d_{xx}F_x n \quad (12)$$

3.2.3 Force and pressure response in piezoelectric sensor

The ability to measure Force and pressure from a sensor is an intricate part of biomedical signal processing. The sensitivity of most sensors (Force, pressure) is dependent on its elastic response from the deformation of its internal structure and arrangement. The output signal produced from a piezoelectric pressure sensor is directly proportional to the applied Force on its thin metal membrane and can be represented in the form of a charge Q . Regtien, P. and Dertien, E. [81] described the two ways charge signal from a piezoelectric sensor can be measured using different electrical elements. The sensor impedance behaves as a capacitance C_e , corresponding

to the electrical capacity of a flat-plate capacitor with (piezoelectric) dielectric. This simple impedance model can be extended by a resistance R_s , modelling leakage currents, and the first method is based on the relation between charge and voltage over a capacitor: $Q=C \cdot V$. Hence the interface_circuit consists of a voltage amplifier. In the second method, the charge can flow through an impedance, preferably a capacitor. The voltage across this capacitor is proportional to the charge, and this type of interface is commonly called a charge amplifier or charge–voltage converter [81].

3.2.4 Design of the piezoelectric sensor based on the PZT

As described above, a PZT pressure sensor generates an electric charge on its electrodes from an applied force. Hence, we can determine the charge generated on the electrodes depending we know the piezoelectric coefficient of the material and material and the Force applied.

We can determine the pressure exerted on the surface area $A_1 = 10 \text{ mm}^2$ ($l=c$) of a PZT sensor according to Figure 16.

Electrodes containing voltage $U = 3 \text{ V}$.

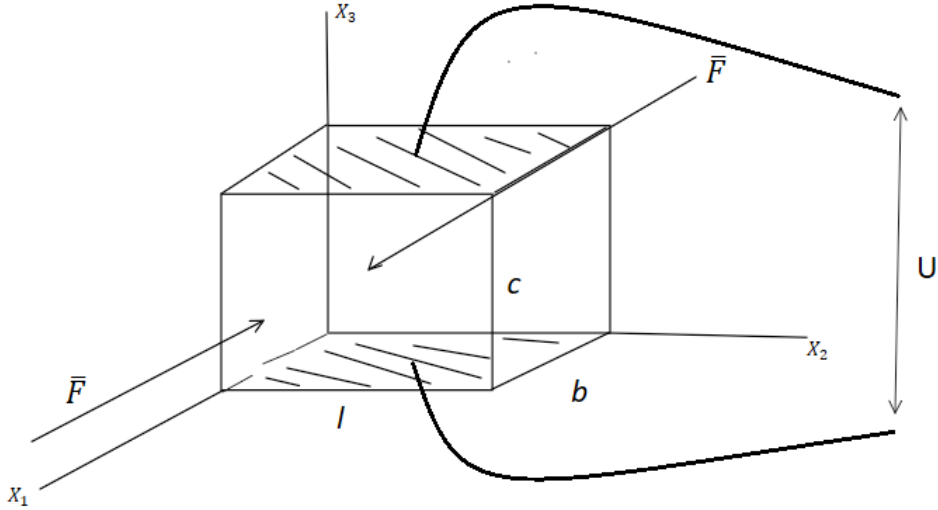
Material properties of piezoelectric ceramic type PZT: compressive strength of $294 \times 10^6 \text{ Pa}$, Relative permittivity $\epsilon_r = 320$,

Piezoelectric coefficient of ceramic PZT:

$$d_{31} = -10 \times 10^{-12} \text{ mV}^{-1}$$

$$d_{33} = 20 \times 10^{-12} \text{ mV}^{-1}$$

Figure 16: Applied force/pressure on a PZT sensor



The electric displacement resulted from the applied force on the surface of the sensor

$$D_i = d_{i\lambda}T_\lambda + \varepsilon_{ij}E_j, \quad (13)$$

where $\lambda = 1-6, j = 1-3,$

where D_i electric displacement [Cm^{-2}], $d_{i\lambda}$ piezoelectric coefficient, T_λ stress component [Nm^{-2}], ε_{ij} permittivity and E_j electric field component.

In its basic

$$D_i = d_{31}T_1$$

The charge on the surface of the sensor $A_1 = l b$ ($l=b$)

$$Q = d_{31}T_1A_1$$

$$Q = d_{31}F_1$$

Using the relationship for a static capacitor sensor (capacitor between electrodes)

$$C = \frac{Q}{U} \quad (14)$$

The resulting charge will be

$$Q = U \varepsilon_o \varepsilon_r A1$$

The force F_1 [N] applied on the surface of the sensor with an area

$A1 = l \cdot c = 0.0001 \text{ m}^2$ ($l=b=c$) in the direction x_1 :

$$F_1 = \frac{U \varepsilon_o \varepsilon_r A1}{d_{31}} = -9.8 \text{ N}$$

Pressure $P = \frac{F}{A1} = 98 \text{ kPa}$.

4. EXPERIMENTAL PART

4.1 Piezoelectric properties of the PZT ceramics

The Lead zirconate titanate ($\text{Pb}[\text{Zr}(x)\text{Ti}(1-x)]\text{O}_3$) PZT for short has a cubic perovskite structure above the curie temperature with the A-site occupied by zirconate and titanate while the B-site by lead. However, the unique properties of their dielectric, piezoelectric and electromechanical coupling factor (table 3) that show anomalous behaviour near MPB make them a preferable option for use in devices to produce ultrasounds transducers, ceramic capacitors, and other sensors and actuators. The performance of PZT ceramics is primarily dependent on the type of material, the chemical composition which varies significantly from one manufacturer to another. The highest piezoelectric properties are obtained around the MPB (approximately 52% PbZrO_3) also, depending on the thickness in material component and single grain layer of a ceramic, one can distinguish a piezoceramic as thin-film, thick-film, or bulk components [82].

- I. Thin-film component – component of thickness ≤ 1 micrometre.
- II. Thick-film component – component of thickness 1 -100 micrometre.
- III. Bulk component – component of thickness ≥ 100 micrometre

The piezoelectric charge constant $d_{ijk} = d_{i\lambda}$ varies based on the coefficient (d_{11} , d_{22} , d_{33} , d_{26} , d_{34} , d_{35} , etc.) and from one PZT ceramic to another. According to CENELEC standard for piezoelectric charge coefficient d_{33} has for hard PZT (type I for American standard of type 100 European standard) 250×10^{-12} C/N, soft PZT (type II or type 200) 4000×10^{-12} C/N.

4.2 Laboratory verification of the basic properties of selected smart materials

4.2.1 Sample materials tested

The tested sample materials used were an APC850 lead zirconate titanate (PZT) disc shape with a diameter of 20 mm and a thickness of 0.8 mm. The alpha quartz disc shape was the other sample material used. Table 3 shows the basic properties of these two sample materials stating their curie temperature and piezoelectric charge and voltage coefficients.

Table 3: Basic material properties of the measured samples

Samples	Materials	Curie temperature T_c [°C] or structure phase transition T_s [°C]	Coupling Factor	Piezoelectric charge coefficient d_{33} [pC/N]	Piezoelectric voltage coefficient g_{33} [mV.m/N]
No.1 PZT Disc shape sample, diameter 20mm/ thickness 0.8mm	APC 850 [83]	$T_c = 360$	$k_{33} 0.72$	400	26
No.2 Quartz Disc shape sample	Quartz Alpha [84]	$T_s = 573$	$k_{11} 0.1$	$d_{11} = 2.31$ [pC/N]	$-98.70 \cdot 10^3$ [m ² C ⁻¹]

4.2.2 Measurement chain

A general measurement chain was established before the experiment. A measurement chain is not only a form of data acquisition, but it also describes the steps followed to get a required result. The sensor is first attached to an amplifier which amplifies the generated charge and is in turn connected to a measurement circuit/analyser (A/D conversion). The resulting output signals are processed on a laptop PC for graphical representation and evaluation.

Figure 17: Measurement chain

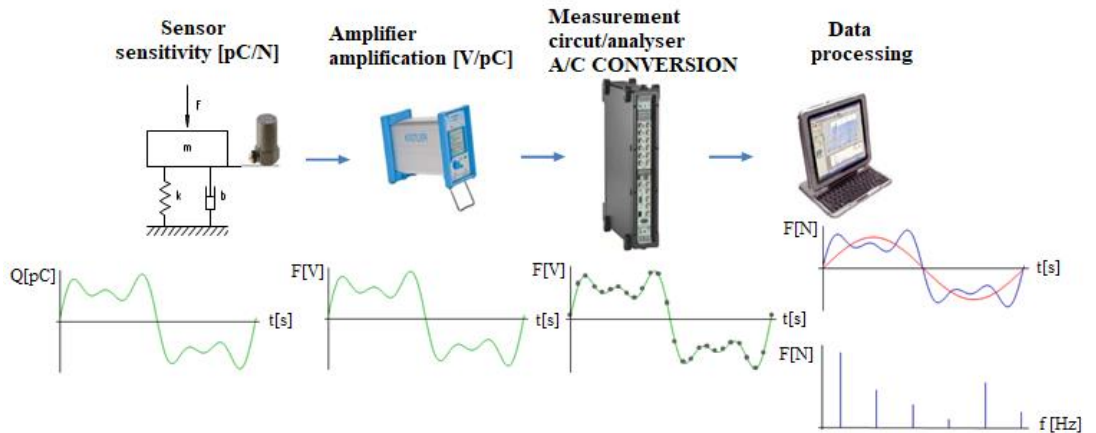
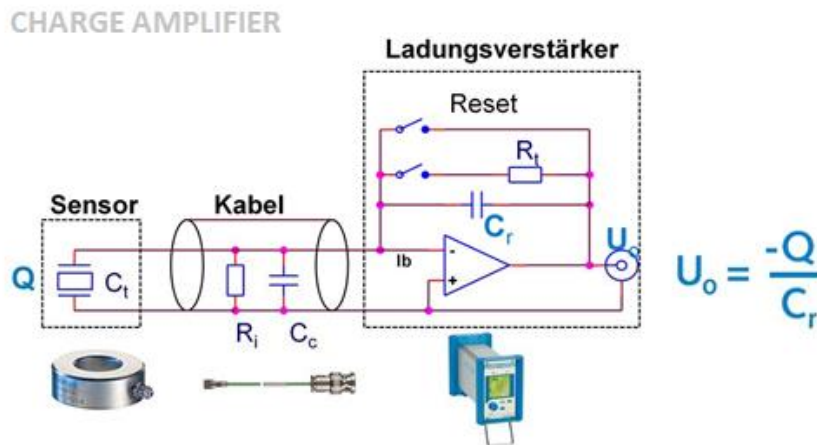


Figure 17 displays a step by step analogy; we explore when experimenting with the two calibration systems in determining the sensitivity of the PZT disc shape pressure sensor and the Quartz disc.

4.2.3 Operation of the charge amplifier

Figure 18: Charge amplifier



The charge amplifier works by converting the electrical input charge generated on the surface of the sensor into a proportional output voltage rather than amplifying it. In other words, the charge amplifier converts an electrical input charge Q into a usable proportional output voltage U_o . In this case, the amplifier acts as a charge integrator by continually compensating for the electric charge generated from the sensor with a magnitude of equal charge and opposite in polarity on the range capacitor. It usually comprises of an inverting voltage amplifier with a high open-loop gain. In order to create high insulation resistance and a minimum leakage in current, capacitive negative feedback is used. Neglecting R_t and R_i , the resulting output voltage U_o will be:

$$U_o = \frac{-Q}{C_r} \cdot \frac{1}{1 + \frac{1}{AC_r} (C_t + C_r + C_c)} \quad (15)$$

Considering the open-loop gain to be sufficiently high, $\frac{1}{AC_r}$ will approach a zero value hence, neglecting the capacitance within the cable and sensor. Therefore, the output voltage will only be dependent on the input charge and range capacitance.

$$U_o = \frac{-Q}{C_r} \quad (16)$$

4.2.4 The methodology of Calibrated systems

The experiment for this bachelor thesis was done at VÚTS a.s in Liberec. It took place in their measurement laboratory under the supervision of my supervisor and Martin Pustka, PhD.

The measurements were done to verify the basic properties of selected smart materials, PTZ APC 850 disc, and Quartz α .

4.2.4.1 Static calibration system

The sensitivity of a sensor in a static system could be measured by the ratio of applied force and charge yield. Using the principle for the creation of a direct piezoelectric effect described on pages 43 and 44 in this thesis, we tested the sensitivity of the PZT APC 850 disc shape sensor and verified its basic properties.

The PZT APC 850 disc shape sensor was attached to two metallic Cu plates and connected to the Kistler 5015 charge amplifier that detects and amplifies the electrical charge created by loading the two metallic Cu plates containing the piezoelectric PZT body, and weights. The amplified charge signals generated was in turn, converter to an output voltage by the charge amplifier. The output signals were processed and evaluated using a multifunctional B&K PULSE on laptop PC.

Figure 19: Setup before static measurement

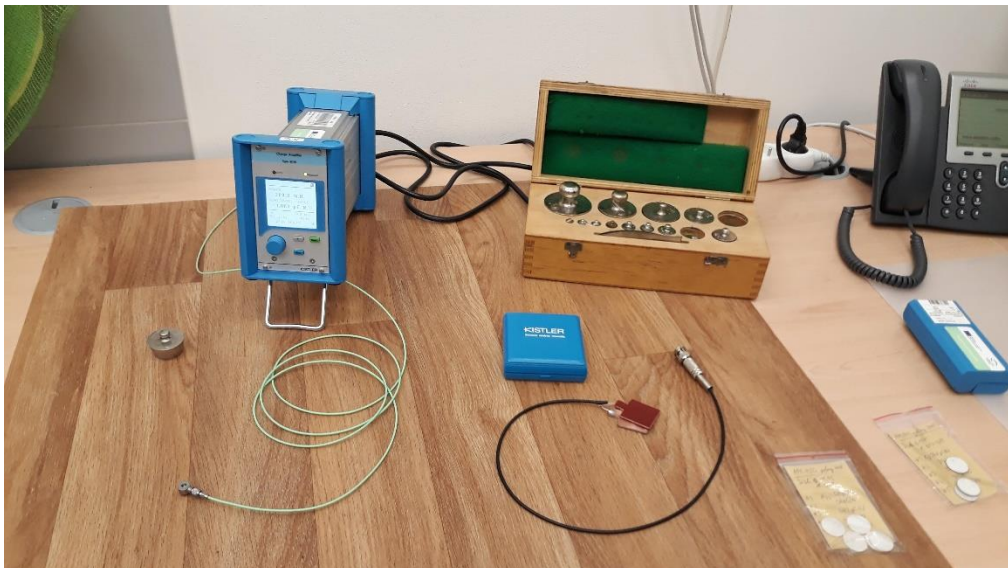


Figure 19 shows the setup before static calibration measurement with the charge amplifier, PZT APC 850 disc shape sensor, and weights.

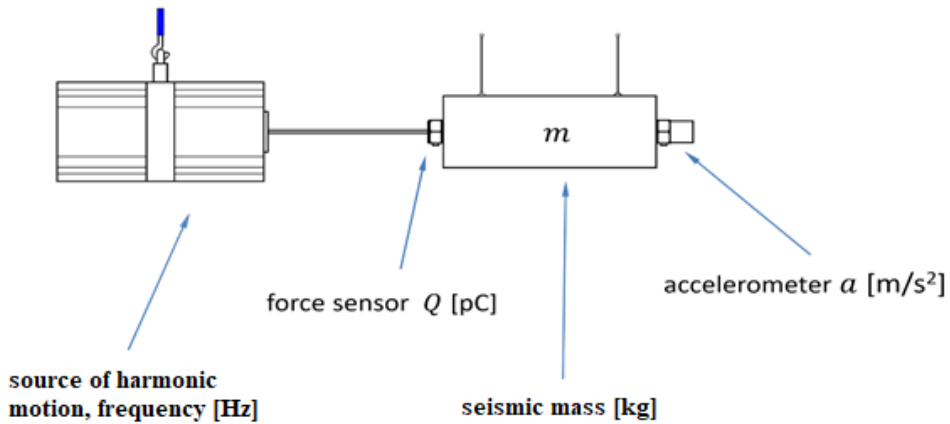
Theoretically, the expected result is supposed to show a direct relationship between the applied force and the output of the electrical charge. With these two quantities, we

could be able to determine the sensitivity level of the sensor and verify its other essential properties.

4.2.4.2 Dynamic calibration system

Unlike the static system used in verifying the properties of PZT APC 850 disc shape sensors, the dynamic calibration system, on the other hand, determines the sensitivity in a quartz crystal relative to frequency in the acceleration of a mass beam as seen in Figure 21.

Figure 20: Dynamic calibration system



$$\text{Dynamic force} \quad F = ma \text{ [N]} \quad (17)$$

$$\text{Sensor sensitivity} \quad S = \frac{Q}{F} \text{ [pC/N]} \quad (18)$$

In this case, I used the principle of the inverse piezoelectric effect described on pages 43 and 44. The Kistler 9212 quartz load cell is connected to an electrodynamic modal exciter type 4825 that produces a harmonic motion of frequency f [Hz] and attaching it to a force sensor charge to CCLD converter type 2647 that produces a charge Q [pC]. This setup was, in turn, attached to a seismic beam with mass m [kg] to which a miniature piezoelectric CCLD accelerometer with an insulated base and cable that

produces an acceleration a [m/s²]. Cables from the CCLD converter and accelerometer were connected to an A/D converter that converts the signals generated from an analogue to digital. These signals generated were further processed using a multifunctional B&K PULSE, which contains a software PULSE LabShop with pulse basic electroacoustic software. An increase in the harmonic frequency will result in an increased acceleration. Using *Newton's first law of motion*, we calculated the force applied for every input charge.

Figure 21 shows the setup of the dynamic measurement, while Figure 22 shows an image of me taking measurements.

Figure 21: Experimental setup for dynamic calibration

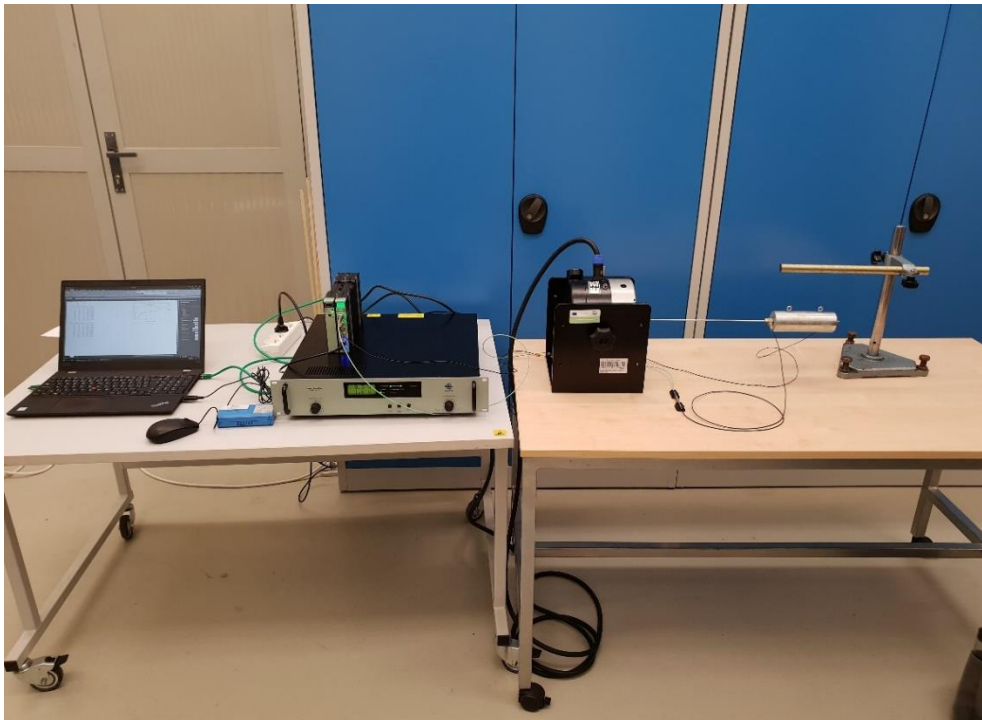


Figure 22: Taking measurement



4.2.5 Experimental result

Two sets of experiments were done using dynamic calibration in determining the sensitivity. The mass of the seismic beam $m = 2.22$ kg

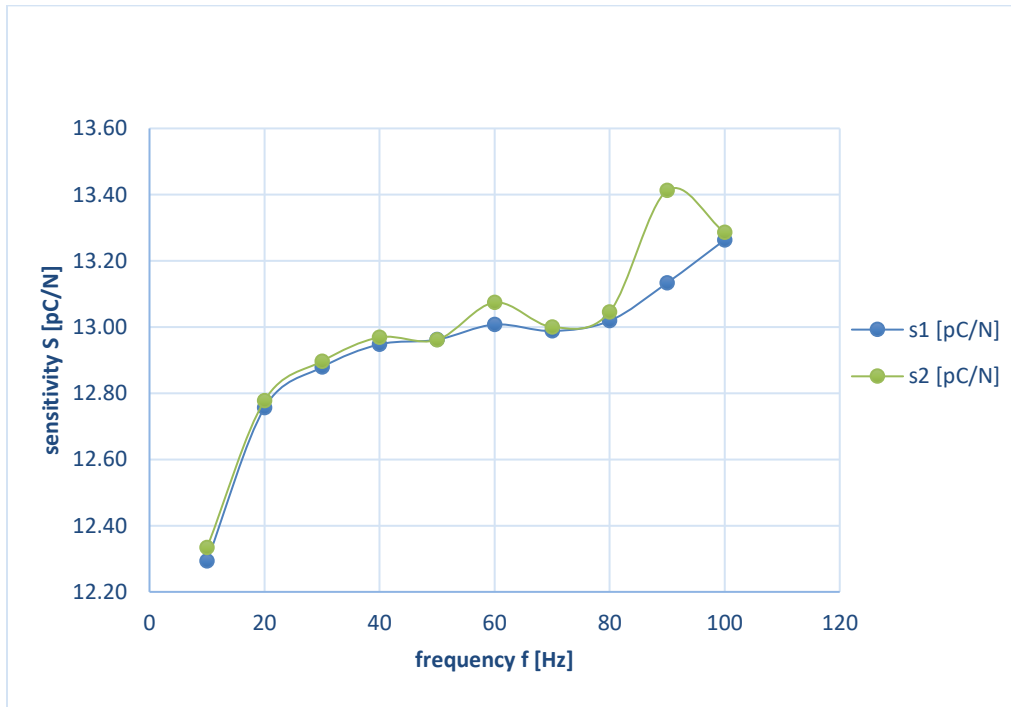
Table 4: Measurement No.1 on the quartz force sensor

f [Hz]	Q [pC]	a [m/s ²]	F [N]	S [pC/N]
10	52.4	1.92	4.26	12.29
20	64.0	2.26	5.02	12.76
30	62.9	2.20	4.88	12.88
40	59.5	2.07	4.60	12.95
50	56.4	1.96	4.35	12.96
60	54.0	1.87	4.15	13.01
70	51.9	1.80	4.00	12.99
80	50.0	1.73	3.84	13.02
90	48.4	1.66	3.69	13.13
100	47.7	1.62	3.60	13.26

Table 5: Measurement No.2 on the quartz force sensor

f [Hz]	Q [pC]	a [m/s ²]	F [N]	S [pC/N]
10	115	4.20	9.32	12.33
20	139	4.90	10.88	12.78
30	138	4.82	10.70	12.90
40	131	4.55	10.10	12.97
50	122	4.24	9.41	12.96
60	119	4.10	9.10	13.07
70	114	3.95	8.77	13.00
80	106	3.66	8.13	13.05
90	106	3.56	7.90	13.41
100	105	3.56	7.90	13.29

Figure 23: Graph of sensitivity vs frequency for measurements No: 1 and 2



4.3 Signal processing and signal evaluation

The laboratory provided a multifunctional B&K PULSE containing a software PULSE LabShop with pulse basic electroacoustic software for the processing of the input and output signals generated during the measurement. The A/D converter was connected to the laptop PC containing the software. The converter converts analogue signals generated from the accelerometer corresponding to the frequency in vibration and transforms it into output value recorded as sensitivity. The software provides accurate measurement even in noisy environments and contains multiple input channels for electrical and acoustic measurements.

It provides analysis using Fast Fourier Transformation (FFT), Steady-State Response (SSR), Time State Response (TSR). It also has an automated procedure for calibration and verification of the normal sensitivity of transducers.

Pulse basic electroacoustic software enables measurement of the output response and frequency response of electroacoustic transducers such as microphones and speakers [85]. The software has a range of additional software including Pulse SSR Analysis Harmonic Distortion BZ-5548, Pulse SSR Analysis Intermodulation Distortion BZ-5549, Pulse SSR Analysis Difference Frequency Distortion BZ-5550, Pulse Directive, and Polar plot BZ-5551, Pulse Sequencer BZ-5600, Pulse Data Manager for electroacoustic Application BZ-5601, Pulse Thiele Small Parameter calculation BZ-5604 and Pulse TSR Analysis - Harmonic Distortion BZ-5742.

In the case of my experiment, I used the built-in Pulse SSR Analysis Difference Frequency Distortion BZ-5550, which enables measurement of different frequency distortion using the steady-state response analyser [85]. It allows the user to calibrate the frequency range according to the type measurements and required outcomes.

Figure 24: Interfacing a piezoelectric sensor: (A) voltage amplifier and (B) charge amplifier [81].

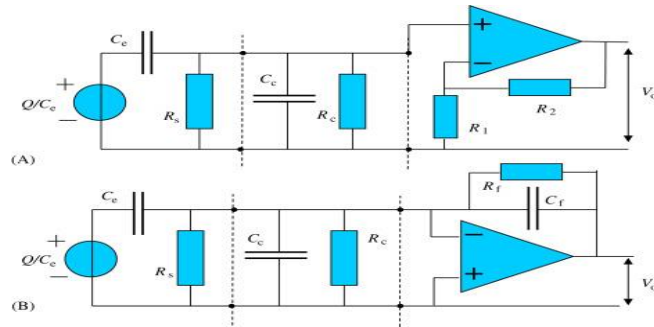


Figure 25 shows examples of these interface circuits, together with models for the sensor and the connecting cable (the part between the dotted lines). It is shown that the cable capacitance can have a substantial influence on the signal transfer of the system due to the capacitive character of the sensor [81], and using the operational amplifier formula, we can derive both the interface circuit and total signal transfer.

4.4 Experimental analysis

4.4.1 Results analysis

The primary goal of this thesis was to test the sensitivity of selected pressure sensors that could be applied in future work to monitor respiratory rate. However, to do so, I first had to determine the type of available piezoelectric material that is sensitive and effective enough in detecting signals of low frequency during measurement.

Tables 4 and 5 show data from measurements using the inverse piezoelectric effect with a dynamic system calibration. A disc-shaped alpha quartz crystal was used and tested twice. The force generated within the sensor was determined by multiplying the output signal generated by the accelerometer with the mass of the seismic beam. i.e, for a frequency of 10 Hz that produces a charge of 52.4 pC from the first sets of measurement, the seismic beam accelerated for 1.92 ms^{-2} . Using Eq. 17, I could calculate for $F = 4.26 \text{ N}$, as shown in Table 4.

Using Eq. (18) I could then calculate for the sensitivity of the material, as shown both in Tables 4 and 5.

Figure 23 gives a graphical representation of frequency plotted against the sensitivity. Based on the graph, there is a consistent increase in sensitivity with an increase in the charge frequency on the quartz disc.

Using descriptive analysis for analysing the result, I found out the mean sensitivity for measurement no:1 was 12.92 and 12.98 pC/N respectively with a standard deviation of 0.26 and 0.29 at 95% confidence interval as well.

The line on the graph could best be used in discussing the sensitivity, output linearity, precision, and accuracy of the sensor material.

4.4.2 Limitations

Several factors limited the entire experiment; precisely, by time and the quarantine lockdown due to Coronavirus (COVID-19) pandemic. It was prohibited to access the laboratory in the L-building (CxI) and its surrounding facilities at the Technical University of Liberec. However, I was able to conduct the experiments in the shortest window of opportunity I had. Thanks to my supervisor, together with Martin Pustka, PhD of the measurement department at VÚTS Liberec, who facilitated the use of their laboratory to do necessary measurements.

Furthermore, I proposed the selection of three different smart materials with piezoelectric properties for the experiment, which include piezoelectric ceramic (PZT), quartz, and relaxor materials. However, due to the expensive nature and unavailability of relaxor materials, I had to limit the experiment only to PZT ceramics and quartz.

Other speculated factors that may have affected the results include temperature, acoustic signals from the surrounding environments, instability in the desk on which the experiment was set up.

5. DISCUSSION

I could only publish the results for the dynamic system calibration measurements for Quartz α . The reason is that the results gained from the static measurement were inconsistent and did not correspond to the expected result. Whenever I applied pressure to the APC 850 piezoelectric disc-shaped sensor, there was an instantaneous drop in the charge created, and it happened consistently throughout the measurement. Even though I could detect the presence of charges, however, they were consequently lost, resulting in the loss of data. For this reason, I decided to use a dynamic system calibration. However, this system works better with a piezoelectric accelerometer, which fits better with the disc Quartz α sample.

The discussion of the results is done relative to the piezoelectric properties of smart materials.

Sensitivity: The charge out from a piezoelectric accelerometer could either be regarded as a voltage or charge source with high impedance. Hence, the charge or voltage sensitivity could be used in describing the relationship between output and acceleration. The piezoelectric accelerometer used for measurement has a normal factory sensitivity (at 159.2 Hz and 4 mA current supply) of 12.2 pC/N with a margin of error $1 \pm 2\%$ [86]. From the descriptive analysis of the result stated on page 61, sensitivity from measurement no:1, 2 were 12.92 and 12.98 pC/N, respectively, which lies within the manufacturer's value. Typically, the sensitivity of a piezoelectric accelerometer decreases over time, and it is necessary to be recalibrated to ensure accuracy.

Output linearity: It is based on the graphical representation; there is a non-linear output in the sensors.

Precision: The result showed in Tables 4, and 5 shows that the measurement was precise and repetitive. I had almost the same value for sensitivity in both measurements for each frequency value. It is important to note that a precise experiment may not necessarily be accurate.

Accuracy: The higher the accuracy, the lower the error, and from our result, I had an error in measurement No:1, 2 at 0.72, and 0.76, respectively, at a 95% confidence interval. It is done by subtracting the measured value from the true value (manufacturers value). This value is below the $1 \pm 2\%$ error stated by the manufacturer.

The piezoelectric properties of smart materials are generally influenced by physical influences, such as temperature, high electric field, high mechanical stress or prestressing, acoustic pressure, etc. Considering that I was unsuccessful at getting measurement values for the APC 850 disc-shaped sensor, I can only speculate on the reasons or say that it may have been due to the factors listed above. My speculation may be that we used the wrong experimental setup to test the APC 850 sensor, or the sensor was not correctly positioned on the Cu plate, or also, the Cu plate was not working correctly.

However, with the dynamic system, the experiment needs to be performed repeatedly or multiple times in order to reduce errors and increase accuracy.

6. CONCLUSION

In principle, it can be concluded that the goals set out in this piece of work have been met.

Ad 1) A detailed search for respiratory monitoring (MRR) and RIP was performed, considering different types of sensors suitable for such measurements.

Ad 2) The comparison of the properties of selected intelligent sensors and materials was performed considering their accuracy, output linearity, range, sensitivity, precision.

Ad 3) The applied force on a sensor made of PZT material was calculated using a defined output voltage from the sensor.

Ad 4) The experimental part was interrupted by the coronavirus crisis. The considered laboratory at the university (CxI) was closed, and the other suitable workplace for necessary measurements on the sensor (VÚTS Liberec) was also quarantined for a substantial period. However, samples of PZT ceramics (manufactured by APC 850, $k_{31} = 0.72$), and a sample of a quartz sensor (Kistler, $k_{11} = 0.1$) was investigated.

The results showed a large scatter of the output charge values for the APC 850 sample, caused by the connection of the measuring circuit. In this case, a static method of determining the piezoelectric coefficient was used. The quartz-based sensor, which was investigated in the dynamic mode showed far more stable values for different frequencies. It is sensitive enough to detect movement with frequencies as low as 10 Hz.

I can conclude that the quartz-based sensor could be the preferable sensor in the application in monitoring respiratory rate. Considering the electromechanical coupling coefficient (and thus the high sensitivity of the sensor), the $\text{Pb}(\text{Mg}_{1/3}\text{Nb}_{2/3})\text{O}_3$ - PbTiO_3 (PMN-PT) relaxor with the giant electromechanical response would be the most suitable from the family of smart materials. However, due to the price, such a sample was not available at that time.

Future work

Through the verification of the sensor and its properties, future work could be focused on exploring its application in monitoring respiratory rate.

References

- [1] J. F. Fieselmann, M. S. Hendryx, C. M. Helms and D. S. Wakefield, "Respiratory rate predicts cardiopulmonary arrest for internal medicine inpatients," *Journal of General Internal Medicine*, vol. 8, no. 7, pp. 354-360, 1993.
- [2] C. P. Subbe, R. G. Davies, E. Williams, P. Rutherford and L. Gemmell, "Effect of introducing the Modified Early Warning score on clinical outcomes, cardio-pulmonary arrests and intensive care utilisation in acute medical admissions*," *Anaesthesia*, vol. 58, no. 8, pp. 797-802, 2003.
- [3] P. Jurak, J. Halamek, V. Vondra, P. Kruzliak, V. Sramek, I. Cundrle, P. Leinveber, M. Adamek and V. Zvoniccek, "Respiratory induced heart rate variability during slow mechanical ventilation," *Wiener klinische Wochenschrift*, vol. 129, no. 7-8, pp. 251-258, 2017.
- [4] R. G. Norman , M. M. Ahmed, J. A. Walsleben and D. M. Rapport, "Detection of respiratory events during NPSG: nasal cannula/pressure sensor versus thermistor," *Sleep*, vol. 20, pp. 1175-1185, 1997.
- [5] G. Roopa Manjunatha, K. Rajanna, D. R. Mahapatra, M. M. Nayak, U. M. Krishnaswamy and R. Srinivasa, "Polyvinylidene fluoride film based nasal sensor to monitor human respiration pattern: An initial clinical study," *Journal of Clinical Monitoring and Computing*, vol. 27, no. 6, pp. 647-657, 2013.
- [6] M. Kotová, J. Kolářová, L. Žalud and P. Dobšák, "Monitorování dechu pomocí tlakových," *Elektrorevue - Internetový časopis*, vol. 15, no. 5, pp. 182--186, 2014.
- [7] R. G. Manjunatha, N. Ranjith, Y. V. Meghashree, K. Rajanna and D. R. Mahapatra, "Identification of different respiratory rate by a piezo polymer based nasal sensor," *2013 IEEE SENSORS*, pp. 1-4, 2013.
- [8] S. Hamdani and A. Fernando, "The Application of a Piezo-Resistive Cardiorespiratory Sensor System in an Automobile Safety Belt," *Sensors*, vol. 15, no. 4, pp. 7742-7753, 2015.

- [9] M. Folke, L. Cernerud, M. Ekström and B. Hök, "Critical review of non-invasive respiratory monitoring in medical care," *Medical & Biological Engineering & Computing*, vol. 41, no. 4, pp. 377-383, 2003.
- [10] A. Hristara-Papadopoulou, J. Tsanakas, G. Diomou and O. Papadopoulou, "Current devices of respiratory physiotherapy," *Hippokratia*, vol. 12, no. 4, p. 211-220., 2008.
- [11] Z. Zhang, J. Zheng, H. Wu, W. Wang, B. Wang and H. Liu, "Development of a Respiratory Inductive Plethysmography Module Supporting Multiple Sensors for Wearable Systems," *Sensors*, vol. 12, no. 10, pp. 13167-13184, 2012.
- [12] P.-Y. Carry, P. Baconnier, A. Eberhard, P. Cotte and G. Benchetrit, "Evaluation of Respiratory Inductive Plethysmography," *Chest*, vol. 111, no. 4, pp. 910-915, 1997.
- [13] S. Liu, R. X. Gao, D. John, J. Staudenmayer and P. Freedson, "Tissue Artifact Removal from Respiratory Signals Based on Empirical Mode Decomposition," *Annals of Biomedical Engineering*, vol. 41, no. 5, pp. 1003-1015, 2013.
- [14] Y. Retory, P. Niedzialkowski, C. de Picciotto, M. Bonay and M. Petitjean, "New Respiratory Inductive Plethysmography (RIP) Method for Evaluating Ventilatory Adaptation during Mild Physical Activities," *PLOS ONE*, vol. 11, no. 3, p. e0151983, 2016.
- [15] A. Waugh and A. Grant, *Ross & Wilson anatomy and physiology in health and illness*, Edinburgh: Elsevier, 2018.
- [16] E. N. Marieb, *Human anatomy & physiology*, San Francisco: Benjamin Cummings, 2001.
- [17] H. H. Dukes, W. O. Reece, H. H. Erickson, G. Goff and E. E. Uemura, *Dukes' physiology of domestic animals*, Ames, Iowa: John Wiley & Sons Inc., 2015, p. 213.
- [18] T. Daiana da Costa, M. de Fatima Fernandes Vara, C. Santos Cristino, T. Zoraski Zanella, G. Nunes Nogueira Neto and P. Nohama, "Breathing Monitoring and Pattern Recognition with Wearable Sensors," *Wearable Devices - the Big Wave of Innovation*, 2019.

- [19] R. Parkes, "Rate of respiration: the forgotten vital sign," *Emergency Nurse*, vol. 19, no. 2, pp. 12-17, 2011.
- [20] W. Buhre and R. Rossaint, "Perioperative management and monitoring in anaesthesia," *The Lancet*, vol. 362, no. 9398, pp. 1839-1846, 2003.
- [21] T. Rantonen, J. Jalonen, J. Grönlund, K. Antila, D. Southall and I. Välimäki, "Increased amplitude modulation of continuous respiration precedes sudden infant death syndrome," *Early Human Development*, vol. 53, no. 1, pp. 53-63, 1998.
- [22] E. Helfenbein, R. Firoozabadi, S. Chien, E. Carlson and S. Babaeizadeh, "Development of three methods for extracting respiration from the surface ECG: A review," *Journal of Electrocardiology*, vol. 47, no. 6, pp. 819-825, 2014.
- [23] K. Gupta, A. Prasad, M. Nagappa, J. Wong, L. Abrahamyan and F. F. Chung, "Risk factors for opioid-induced respiratory depression and failure to rescue," *Current Opinion in Anaesthesiology*, vol. 31, no. 1, pp. 110-119, 2018.
- [24] S. S. Weigt, M. Abrazado, E. C. Kleerup, D. P. Tashkin and C. B. Cooper, "Time course and degree of hyperinflation with metronome-paced tachypnea in COPD patients," *COPD*, vol. oct;5, no. 5, pp. 298-304, 2008.
- [25] C. Massaroni, A. Nicolò, D. Lo Presti, M. Sacchetti, S. Silvestri and E. Schena, "Contact-Based Methods for Measuring Respiratory Rate," *Sensors*, vol. 19, no. 4, p. 908, 2019.
- [26] F. AL-Khalidi, R. Saatchi, D. Burke, H. Elphick and S. Tan, "Respiration rate monitoring methods: A review," *Pediatric Pulmonology*, vol. 46, no. 6, pp. 523-529, 2011.
- [27] L. D'Angelo, S. Weber, Y. Honda, T. Thiel, F. Narbonneau and T. Luth, "A system for respiratory motion detection using optical fibers embedded into textiles," *2008 30th Annual International Conference of the IEEE Engineering in Medicine and Biology Society*, pp. 3694-3697, 2008.
- [28] J. FRADEN, *Handbook of modern sensors: physics, designs, and applications*, 4th ed., New York: Springer, 2010.
- [29] K. Jafarian, M. Aminehlami, K. Hassani, M. Kamran, M. N. Lahiji and D. J. Doyle, "A multi-channel acoustics monitor for perioperative respiratory monitoring:

- preliminary data," *Journal of Clinical Monitoring and Computing*, vol. 30, no. 1, pp. 107-118, 2015.
- [30] M. A. E. Ramsay, M. Usman, E. Lagow, M. Mendoza, E. Untalan and E. De Vol, "The Accuracy, Precision and Reliability of Measuring Ventilatory Rate and Detecting Ventilatory Pause by Rainbow Acoustic Monitoring and Capnometry," *Anesthesia & Analgesia*, vol. 117, no. 1, pp. 69-75, 2013.
- [31] J. Cashman and S. Dolin, "Respiratory and haemodynamic effects of acute postoperative pain management: evidence from published data," *British Journal of Anaesthesia*, vol. 93, no. 2, pp. 212-223, 2004.
- [32] M. Patino, D. T. Redford, T. W. Quigley, M. Mahmoud, C. D. Kurth and P. Szmuk, "Accuracy of acoustic respiration rate monitoring in pediatric patients," *Pediatric Anesthesia*, 2013.
- [33] C. Ahlstrom, O. Liljefeldt, P. Hult and P. Ask, "Heart sound cancellation from lung sound recordings using recurrence time statistics and nonlinear prediction," *IEEE Signal Processing Letters*, vol. 12, no. 12, pp. 812-815, 2005.
- [34] J. H. Atkins and J. E. Mandel, "Performance of Masimo Rainbow Acoustic Monitoring for Tracking Changing Respiratory Rates Under Laryngeal Mask Airway General Anesthesia for Surgical Procedures in the Operating Room," *Anesthesia & Analgesia*, vol. 119, no. 6, pp. 1307-1314, 2014.
- [35] J. H. Kim, S. I. Chi, H. J. Kim and K.-S. Seo, "The effect of dental scaling noise during intravenous sedation on acoustic respiration rate (RRa™)," *Journal of Dental Anesthesia and Pain Medicine*, vol. 18, no. 2, p. 97, 2018.
- [36] S. Liehr, P. Lenke, M. Wendt, K. Krebber, M. Seeger, E. Thiele, H. Metschies, B. Gebreselassie and J. Munich, "Polymer Optical Fiber Sensors for Distributed Strain Measurement and Application in Structural Health Monitoring," *Institute of Electrical and Electronics Engineers (IEEE)*, vol. 9, no. 11, pp. 1330-1338, 2009.
- [37] E. Hanada, "The electromagnetic environment of hospitals: how it is affected by the strength of electromagnetic fields generated both inside and outside the hospital," *Ann Ist Super Sanita.*, vol. 43, no. 3, pp. 208-217, 2007.

- [38] M. Krehel, M. Schmid, R. Rossi, L. Boesel, G.-L. Bona and L. Scherer, "An Optical Fibre-Based Sensor for Respiratory Monitoring," *Sensors*, vol. 14, no. 7, pp. 13088-13101, 2014.
- [39] X. Li, D. Liu, R. Kumar, W. P. Ng, Y.-q. Fu, J. Yuan, C. Yu, Y. Wu, G. Zhou, G. Guorui, Y. Semenova and Q. Wu, "A simple optical fiber interferometer based breathing sensor," *Measurement Science and Technology*, vol. 28, no. 3, p. 035105, 2017.
- [40] W. J. Yoo, K. W. Jang, J. K. Seo, J. Y. Heo, J. S. Moon, J. H. Jun, J.-Y. Park and B. Lee, "Development of optical fiber-based respiration sensor for noninvasive respiratory monitoring," *Optical Review*, vol. 18, no. 1, pp. 132-138, 2011.
- [41] A. Ejupi and C. Menon, "Detection of Talking in Respiratory Signals: A Feasibility Study Using Machine Learning and Wearable Textile," *Sensors*, vol. 18, no. 8, p. 2474, 2018.
- [42] J. Daniels and N. Pourmand, "Label-Free Impedance Biosensors: Opportunities and Challenges," *Electroanalysis*, vol. 19, no. 12, pp. 1239-1257, 2007.
- [43] G. Ertürk and B. Mattiasson, "Capacitive Biosensors and Molecularly Imprinted Electrodes," *Sensors*, vol. 17, no. 2, p. 390, 2017.
- [44] T. Reinvuo, M. Hannula, H. Sorvoja, E. Alasaarela and R. Myllyla, "Measurement of respiratory rate with high-resolution accelerometer and emfit pressure sensor," *Proceedings of the 2006 IEEE Sensors Applications Symposium, 2006.*, pp. 192-195 .
- [45] P. W. Rehrig, W. S. Hackenberger, S. E. Park and T. R. Shrout, "Relaxor-based ferroelectric single crystals for electromechanical actuators," in *piezoelectric materials in devices*, Lausanne, EPFL, 2003, pp. 433-454.
- [46] B. R. Eggins, *Chemical sensors and biosensors*, Chichester: J. Wiley, 2010.
- [47] J. J. Carr and J. M. Brown, *Introduction to biomedical equipment technology*, 3rd ed., Upper Saddle River, N.J.: Prentice Hall, 1998.
- [48] I. Smith, J. Mackay, N. Fahrid and D. Kruckeck, "Respiratory rate measurement: a comparison of methods," *British Journal of Healthcare Assistants*, vol. 5, no. 1, pp. 18-23, 2011.

- [49] S. K. Kundu, K. Kumagai and M. Sasaki, "A Wearable Capacitive Sensor for Monitoring Human Respiratory Rate," *Japanese Journal of Applied Physics*, vol. 52, no. 4S, p. 04CL05, 2013.
- [50] B. Jaffe, W. R. Cook and H. Jaffe, *Piezoelectric ceramics*, New York: Academic press INC., 1971.
- [51] J. Scott, "Applications of Modern Ferroelectrics," *Science*, vol. 315, no. 5814, pp. 954-959, 2007.
- [52] B. Jiang, J. Iocozzia, L. Zhao, H. Zhang, Y.-W. Harn, Y. Chen and Z. Lin, "Barium titanate at the nanoscale: controlled synthesis and dielectric and ferroelectric properties," *Chemical Society Reviews*, vol. 48, no. 4, pp. 1194-1228, 2019.
- [53] G. G. Genchi, A. Marino, A. Rocca, V. Mattoli and G. Ciofani, "Barium titanate nanoparticles: promising multitasking vectors in nanomedicine," *Nanotechnology*, vol. 27, no. 23, p. 232001, 2016.
- [54] E. Sun and W. Cao, "Relaxor-based ferroelectric single crystals: Growth, domain engineering, characterization and applications," *Progress in Materials Science*, vol. 65, pp. 124-210, 2014.
- [55] K. Uchino, *Ferroelectric devices*, New York: Marcel Dekker, 2000.
- [56] R. A. Cowley, S. N. Gvasaliya, S. G. Lushnikov, B. Roessli and G. M. Rotaru, "Relaxing with relaxors: a review of relaxor ferroelectrics," *Advances in Physics*, vol. 60, no. 2, pp. 229-327, 2011.
- [57] R. Whatmore, "Ferroelectric Materials," *Springer Handbook of Electronic and Photonic Materials*, pp. 1-1, 2017.
- [58] Y. Liu, H. Aziguli, B. Zhang, W. Xu, W. Lu, J. Bernholc and Q. Wang, "Ferroelectric polymers exhibiting behaviour reminiscent of a morphotropic phase boundary," *Nature*, vol. 562, no. 7725, pp. 96-100, 218.
- [59] S.-E. Park and T. R. Shrout, "Relaxor based ferroelectric single crystals for electro-mechanical actuators," *Materials Research Innovations*, vol. 1, no. 1, pp. 20-25, 1997.

- [60] J. Luo and S. Zhang, "Advances in the Growth and Characterization of Relaxor-PT-Based Ferroelectric Single Crystals," *Crystals*, vol. 4, no. 3, pp. 306-330, 2014.
- [61] H. Uršic and M. Kosec, "Relaxor-ferroelectric PMN–PT Thick Films," in *Ferroelectrics - physical effects*, Rijeka, cInTech, 2011.
- [62] L. Lim, "Single crystal preparation techniques for manufacturing piezoelectric materials," *Advanced Piezoelectric Materials*, pp. 412-440, 2010.
- [63] D. Alikin, A. Turygin, A. Kholkin and V. Shur, "Ferroelectric Domain Structure and Local Piezoelectric Properties of Lead-Free (K_{0.5}Na_{0.5})NbO₃ and BiFeO₃-Based Piezoelectric Ceramics," *Materials*, vol. 10, no. 1, p. 47, 2017.
- [64] D. Fang, F. Li, B. Liu, Y. Zhang, J. Hong and X. Guo, "Advances in Developing Electromechanically Coupled Computational Methods for Piezoelectrics/Ferroelectrics at Multiscale," *Applied Mechanics Reviews*, vol. 65, no. 6, 2013.
- [65] V. Y. Shur and A. R. Akhmatkhanov, "Domain shape instabilities and dendrite domain growth in uniaxial ferroelectrics," *Philosophical Transactions of the Royal Society A: Mathematical, Physical and Engineering Sciences*, vol. 376, no. 2113, p. 20170204, 2018.
- [66] A. A. BOKOV and Z.-G. Ye, "DIELECTRIC RELAXATION IN RELAXOR FERROELECTRICS," *Journal of Advanced Dielectrics*, vol. 02, no. 02, p. 1241010, 2012.
- [67] T.-B. Xu, "Energy harvesting using piezoelectric materials in aerospace structures," *Structural Health Monitoring (SHM) in Aerospace Structures*, pp. 175-212, 2016.
- [68] S. J. Rupitsch, "Piezoelectricity," in *Piezoelectric Sensors and Actuators*, 2018, pp. 43-81.
- [69] J. Kim, H. Takenaka, Y. Qi, A. R. Damodaran, A. Fernandez, R. Gao, M. R. McCarter, S. Saremi, L. Chung, A. M. Rappe and L. W. Martin, "Epitaxial Strain Control of Relaxor Ferroelectric Phase Evolution," *Advanced Materials*, vol. 31, no. 21, p. 1901060, 2019.

- [70] N. Setter, "ABC of piezoelectricity and piezoelectric materials," in *Piezoelectric materials in devices*, Lausanne, EPFL, 2003, pp. 1-28.
- [71] R. Georges Sabat, B. K. Mukherjee, W. Ren and G. Yang, "Temperature dependence of the complete material coefficients matrix of soft and hard doped piezoelectric lead zirconate titanate ceramics," *Journal of Applied Physics*, vol. 101, no. 6, p. 064111, 2007.
- [72] L. Tang, H. Tian, Y. Zhang and W. Cao, "Temperature dependence of dielectric, elastic, and piezoelectric constants of [001]cpoled Mn-doped $0.24\text{Pb}(\text{In}_{1/2}\text{Nb}_{1/2})\text{O}_3\text{-}0.46\text{Pb}(\text{Mg}_{1/3}\text{Nb}_{2/3})\text{O}_3\text{-}0.30\text{PbTiO}_3$ single crystal," *Applied Physics Letters*, vol. 108, no. 8, p. 082901, 2016.
- [73] V. Pushin, N. Kuranova, E. Marchenkova and A. Pushin, "Design and Development of Ti–Ni, Ni–Mn–Ga and Cu–Al–Ni-based Alloys with High and Low Temperature Shape Memory Effects," *Materials*, vol. 12, no. 16, p. 2616, 2019.
- [74] J. Nosek, "Properties of Smart Materials and their use for sensors and actuators 1". *Smart Sensors and Actuators*.
- [75] G. Gaultschi, *Piezoelectric Sensorics*, Springer Berlin Heidelberg, 2002.
- [76] B. Kok, S. Gareh, H. Goh and C. Uttraphan, "Electromechanical-Traffic Model of Compression-Based Piezoelectric Energy Harvesting," *MATEC Web of Conferences*, vol. 70, no. 10007, 2016.
- [77] "<https://en.wikipedia.org/wiki/Quartz>," [Online]. [Accessed 12 04 2020].
- [78] Y. Saigusa, "Quartz-based piezoelectric materials," *Advanced Piezoelectric Materials*, pp. 171-203, 2010.
- [79] J. Tichý, J. Erhart, E. Kittinger and J. Přívratská, *Fundamentals of Piezoelectric Sensorics*, Berlin: Springer Berlin, 2014.
- [80] "www.piceramic.com," [Online]. Available: <https://www.piceramic.com/en/piezo-technology/properties-piezo-actuators/displacement-modes/#c2499>. [Accessed 14 04 2020].

- [81] P. P. L. Regtien and E. Dertien, "Piezoelectric sensors," in *Sensors for Mechatronics*, second edition ed., Elsevier, 2018, pp. 245-265.
- [82] W. W. Wolny, "Application of piezoceramics - The manufacturer perspective," in *Piezoelectric Materials and Devices*, N. Setter, Ed., Lausanne, N. Setter, 2002, pp. 67 - 82.
- [83] V. Giurgiutiu and A. N. Zagrai, "Characterization of Piezoelectric Wafer Active Sensors," *Journal of Intelligent Material Systems and Structures*, vol. 11, no. 12, pp. 959-976, 2000.
- [84] J. ZELENKA, *Piezoelectric Resonators and their Applications*, Amsterdam: Academia Prague, Elsevier Science Publishers, 1986.
- [85] "Briel & Kjaer- sound and vibration measurement," 2015. [Online]. Available: <https://www.bksv.com/en/products/Analysis-software/acoustic-application-software/electroacoustic-device-testing-software/pulse-basic-electroacoustics-7797>. [Accessed 24 6 2020].
- [86] "www.kistler.com," 2015. [Online]. Available: <https://www.bksv.com/-/media/literature/Product-Data/bp2051.ashx>. [Accessed 2020 6 22].

Appendix

Appendix No. 1 CCLD Accelerometer Type 4394, Kistler, 2020

Appendix No. 2 Descriptive statistics of measured results




Appendix No. 3 Characterisation of Piezoelectric Water Active Sensors (APC850), 2020

Appendix-1

Specifications – Types 4394 and 4397-A			
Type No.		4394 [*]	4397-A [*]
General			
Weight (excluding cable, wherever applicable)	gram	2.9	2.4
	oz	0.102	0.085
Voltage Sensitivity (at 159.2 Hz and 4 mA supply current)	mV/ms ⁻²	1 ±2%	
	mV/g	9.8 ±2%	
Frequency Range	Amplitude (±10%)	1 to 25000	
	Amplitude (±5%)	1 to 10000	
	Phase (±5°)	4 to 2500	
Mounted Resonance Frequency	kHz	52	53
Max. Transverse Sensitivity (at 30 Hz, 100 ms ⁻²)	%	<4	
Transverse Resonance Frequency	kHz	15	17
Measuring range (± peak)	kms ⁻²	5 (7.5 when T <100 °C)	
	g	500 (750 when T <100 °C)	
TEDS		No	
Electrical			
Bias Voltage	at 25 °C and 4 mA	V	
	at full temp. and curr. range	12 ±0.5 8 to 15	
Power Supply	Constant current	mA	
	Unloaded supply voltage	V	
Output Impedance	Ω	100	
Start-up time (to final bias ±10%)	s	<5	
Residual Noise (inherent RMS broadband noise in the specified frequency range)	μV	<25	<15
	μg	<2500	<1500
Noise Spectral	10 Hz	1.3 (130)	0.79 (79)
	100 Hz	0.45 (45)	0.21 (21)
	1000 Hz	0.17 (17)	0.14 (14)
Environmental			
Operating Temperature Range	°C	-50 to +125	
	°F	-58 to +257	
Temperature Coefficient of Sensitivity	%/°C	0.04	0.05
Temperature Transient Sensitivity (3 Hz Lower Limiting Freq. -3 dB, 6 dB/oct)	ms ⁻² /°C	2	
	g/°F	0.11	
Magnetic Sensitivity (50 Hz, 0.038 T)	ms ⁻² /T	10	50
	g/kGauss	0.1	0.5
Base Strain Sensitivity (at 250 με in base plane)	ms ⁻² /με	0.005	
	g/με	0.0005	
Max. Non-destructive Shock (± peak)	kms ⁻²	100 (axial), 50 (transverse)	
	g	10000 (axial) 5000 (transverse)	
Mechanical			
Case Material		Titanium ASTM Grade 2	
Piezoelectric Sensing Element		PZ 23	
Construction		DeltaShear	
Sealing		Welded	
Electrical Connector		Coaxial M3	
Mounting		M3 × 2 mm threaded hole	M3 × 2.4 mm threaded hole
Mounting Torque	Nm (lb·in)	Max. 0.6 (5.3), Min. 0.2 (1.8)	

^{*} All values are typical at 25 °C (77 °F) unless otherwise specified

COMPLIANCE WITH STANDARDS

CE   

Brüel & Kjær Sound & Vibration Measurement A/S
DK-2850 Naerum - Denmark · Telephone: +45 77 41 20 00 · Fax: +45 45 80 14 05
www.bksv.com · info@bksv.com

Local representatives and service organisations worldwide

Ordering Information

Type 4394

Includes the following accessories:

- Carrying Box
- Calibration Chart
- AO-1381-D-012: Cable M3 (M) to 10–32 UNF (M), 1.2 m, 250 °C (482 °F)
- 3×YS-8321: Steel stud with flange, M3/M3, 3.5 mm

Type 4397

Includes the following accessories:

- Carrying Box
- Calibration Chart
- AO-1381-D-012: Cable M3 (M) to 10–32 UNF (M), 1.2 m, 250 °C (482 °F)
- 4×YS-8321: Steel stud with flange, M3/M3, 3.5 mm

Type 4397-A

Includes the following accessories:

- Carrying Box
- Calibration Chart
- 1×YS-8321: Steel stud with flange, M3/M3, 3.5 mm

Optional Accessories

AO-0283	Super low-noise coaxial cable, M3 to 10–32 UNF, 250 °C (482 °F)
AO-0339	Flexible low-noise coaxial cable, M3 to 10–32 UNF, 250 °C (482 °F)
AO-1381	Flexible double-screened low-noise coaxial cable, M3 to 10–32 UNF, 250 °C (482 °F)
AO-0641	Low-cost coaxial cable, M3 to BNC, 90 °C (194 °F)
AO-0698	Super low-noise coaxial cable, M3 to SMB, 250 °C (482 °F)
UA-0867	25 × cement stud, M3, 8.0 mm dia.
UA-0186	25 × extension connector 10–32 UNF
UA-1075	5 × mounting magnet
UA-1221	25 × steel stud with flange, M3/M3, 3.5 mm
WA-0224	Mechanical filter
JP-0145	Plug adaptor, BNC/10–32 UNF
QA-0041	Tap for M3 thread
QA-0042	Hexagonal key for M3 studs
QS-0007	Tube of cyanoacrylate adhesive
YI-0216	Beeswax for mounting
Type 4397-A only	
UA-1193	10 × insulated stud, M3/M3, 2.4 mm
YQ-2003	M3 threaded steel stud, 5 mm
YQ-2007	M3 threaded steel stud, 8 mm
Calibration Services	
439x-CAF	Accredited calibration
439x-CAI	Accredited initial calibration
439x-CFF	Factory standard calibration
439x-CTF	Traceable calibration

^{*} x = 4 or 7

Brüel & Kjær reserves the right to change specifications without notice. © Brüel & Kjær. All rights reserved.

BP 2051 - 13



Appendix-2:

	S1	S2			S1 [pC/N]	S2 [pC/N]
AVERAGE	12,92	12,98		Mean	12,92	12,98
STANDARD DEVIATION	0,260089	0,290512		Standard Error	0,08	0,09
SAMPLE SIZE	10	10		Median	12,97	12,98
CONFIDENCE COEFFICEINT	1,96	1,96		Standard Deviation	0,26	0,29
MARGIN OF ERROR	0,161205	0,180061		Sample Variance	0,07	0,08
UPPER BOUND	13,09	13,16		Kurtosis	4,00	2,31
LOWER BOUND	12,76	12,80		Skewness	-1,63	-0,90
MAX	13,26	13,41		Range	0,97	1,08
MIN	12,29	12,33		Minimum	12,29	12,33
RANGE	0,97	1,08		Maximum	13,26	13,41
				Sum	129,25	129,76
				Count	10,00	10,00
				Confidence Level(95.0%)	0,19	0,21

SUMMARY
OUTPUT

<i>Regression Statistics</i>	
Multiple R	0,863291
R Square	0,745272
Adjusted R Square	0,713431
Standard Error	16,20767
Observations	10

ANOVA

	<i>df</i>	<i>SS</i>	<i>MS</i>	<i>F</i>	<i>Significance F</i>
Regression	1	6148,491	6148,491	23,40601	0,001291
Residual	8	2101,509	262,6886		
Total	9	8250			

	<i>Coefficients</i>	<i>Standard Error</i>	<i>t Stat</i>	<i>P-value</i>	<i>Lower 95%</i>	<i>Upper 95%</i>	<i>Lower 95.0%</i>	<i>Upper 95.0%</i>
Intercept	-1243,88	268,53	-4,63	0,00	-1863,10	624,66	1863,10	624,66
S1 [pC/N]	100,49	20,77	4,84	0,00	52,59	148,39	52,59	148,39

Appendix-3:

30. 6. 2020

(13) (PDF) Characterization of Piezoelectric Wafer Active Sensors

Characterization of Piezoelectric Wafer Active Sensors

Article

Dec 2000

Download

Property	Unit	Symbol	APC-640	APC-641	APC-880	APC-850	APC-855	APC-856
Relative dielectric constant	1	$\epsilon_{11}, \epsilon_{33}$	1250	1350	1000	1750	3250	4100
Dissipation factor measured C 1 kC@ low field	%	$\tan \delta$	0.4	0.35	0.35	1.4	2	2.7
Curie temperature	$^{\circ}\text{C}$	T_C	325	320	310	360	195	150
Coupling coefficient	1	k_p	0.59	0.60	0.50	0.63	0.65	0.65
		k_{33}	0.72	0.68	0.62	0.72	0.74	0.73
		k_{31}	0.35	0.33	0.30	0.36	0.38	0.36
		k_{15}	0.70	0.67	0.55	0.68	0.66	0.65
Piezoelectric coefficient	10^{-12} C/N or m/V	d_{33}	290	275	215	480	580	620
		$-d_{31}$	125	109	95	175	270	260
		d_{15}	480	450	330	590	720	710
Piezoelectric coefficient	10^{-3} V-m/N or m ² /C	g_{33}	26.5	25.5	25	26	19.5	18.5
		$-g_{31}$	11	10.5	10	12.4	8.8	8.1
		g_{15}	38	35	28	36	27	25
Young's modulus	10^{11} N/m ²	Y_{11}^T	8	7.6	9	6.3	6.1	5.8
		Y_{33}^T	6.8	6.3	7.2	5.4	4.8	4.5
Frequency constants	Hz-m or N m/s	N_L	1524	1700	1725	1500	1475	-
		N_T	2005	2005	2110	2032	1930	1980
		N_R	2130	2055	2080	1980	1980	-
Elastic compliance	10^{-12} m ² /N	S_{11}^T	11.8	11.7	10.8	15.3	14.8	15.0
		S_{33}^T	17.4	17.3	15.0	17.3	16.7	17.0
Density	g/cc	ρ	7.6	7.6	7.6	7.7	7.5	7.5
Mechanical quality factor	1	Q_m	500	1400	1000	80	75	72

Table 3 Peaks of the admittance and impedance real-part plots, numerical simulation of a PZT active sensor with $l = 7$ mm, $b = 1.66$ mm, $t = 0.2$ mm, APC-850 piezoceramic, $\nu = 0.31$

Mode No.	1	2	3	4	5
Slightly damped resonance frequencies, f_r , kHz	208.059	624.17	1040.29	1456.41	1872.54
Undamped resonance frequencies, f_r , kHz	208.056	624.16	1040.28	1456.39	1872.51
Error in f_r vs. f_{r0} , %	0.0014%	0.0016%	0.0016%	0.0014%	0.0016%
Slightly damped anti-resonance frequencies, f_a , kHz	219.89	628.35	1042.84	1458.26	1873.99
Undamped anti-resonance frequencies, f_a , kHz	219.88	628.32	1042.78	1458.18	1873.90
Error in f_a vs. f_{a0} , %	0.0045%	0.0048%	0.0058%	0.0055%	0.0048%

Figure

Caption

Table 2 Properties of piezoelectric ceramic APC-850
(as from the company website
www.americanpiezo.com)

This figure was
uploaded by
[Andrei N Zagrai](#)
Content may be
subject to
copyright.

List of figures

Figure 1: Respiratory inductive plethysmography	18
Figure 2: Structures associated with the respiratory system. [15]	20
Figure 3: Graphical description of Boyle's law.....	22
Figure 4: Breathing process: (a) structures involved in the breathing process; (b) inhalation event; and (c) exhalation event. [18].....	23
Figure 5: Most popular contact-based techniques for measuring RR and related areas of the body on which the sensors must be positioned. PPG = photoplethysmography; ECG = Electrocardiography. [25]	25
Figure 6: The ideal cubic perovskite structure. Large open circles denote the oxygen atoms, smaller open and solid circles denote the metal cations with A and B sites, respectively. [56].....	35
Figure 7: Tertiary phase diagram depicting MPBs in PZT and Relaxor-PT system in piezoelectric ceramics [59]	36
Figure 8: Schematic depiction of a typical domain structure [64]	37
Figure 9: Direct and converse piezoelectric effect [76].....	44
Figure 10: shows the unit cell of α -quartz. Small black circles show the Si atom and the large white circles show the O atom [78].....	45
Figure 11: Single unit of Si and O atoms viewed from the Z-axis [78].....	45
Figure 12: Quartz crystal plate x, y, z plan [78].....	46
Figure 13: X-axis (electric axis) and Y-axis (mechanical axis) are the two-fold symmetry axis [78].	46
Figure 14: Longitudinal piezoelectric effect [78]	48
Figure 15: Transverse piezoelectric effect [78]	49
Figure 16: Applied force/pressure on a PZT sensor.....	52
Figure 17: Measurement chain.....	56
Figure 18: Charge amplifier.....	56
Figure 19: Setup before static measurement	58
Figure 20: Dynamic calibration system	59
Figure 21: Experimental setup for dynamic calibration.....	60
Figure 22: Taking measurement	61
Figure 23: Graph of sensitivity vs frequency for measurements No: 1 and 2.....	62
Figure 24: Interfacing a piezoelectric sensor: (A) voltage amplifier and (B) charge amplifier [81].	64

List of tables

Table 1: Some perovskite and their properties [57]	35
Table 2 Comparison of piezoelectric constants and electromechanical coupling factors of conventional piezoelectric and ferroelectric materials. [54]	41
Table 3: Basic material properties of the measured samples	55
Table 4: Measurement No.1 on the quartz force sensor.....	61
Table 5: Measurement No.2 on the quartz force sensor.....	62